Seismotectonics of the Southern Apennines and Adriatic foreland: insights on active regional E-W shear zones from analogue modeling

Daniela Di Bucci (1), Antonio Ravaglia (2, 3), Silvio Seno (2), Giovanni Toscani (2), Umberto Fracassi (4), Gianluca Valensise (4)

1) *Dipartimento della Protezione Civile, Servizio Sismico Nazionale. Via Vitorchiano, 4 - 00189 Roma, Italy*
2) *Dipartimento di Scienze della Terra, Università di Pavia. Via Ferrata, 1 - 27100 Pavia, Italy*
3) *now at Midland Valley Exploration Ltd. 14 Park Circus - G3 6AX Glasgow, UK*
4) *Istituto Nazionale di Geofisica e Vulcanologia, Via di Vigna Murata, 605 - 00143 Roma, Italy*

Corresponding Author:
Daniela Di Bucci
Dipartimento della Protezione Civile
Servizio Sismico Nazionale
Via Vitorchiano, 4
00189 - Roma, Italy
Tel.: ++39-06-68204761
Fax: ++39-06-68202877
e-mail: daniela.dibucci@protezionecivile.it

Running title: Active shear zones: analogue modeling

Index Terms: 7230 Seismicity and tectonics. 8010 Fractures and faults. 8011 Kinematics of crustal and mantle deformation. 8111 Continental tectonics: strike-slip and transform. 8123 Dynamics: seismotectonics.

Keywords: Active strike-slip fault, sandbox model, Southern Italy.

Abstract: The active tectonics at the front of the Southern Apennines and in the Adriatic foreland is characterized by E-W striking, right-lateral seismogenic faults, interpreted as reactivated inherited discontinuities. The best studied among these is the Molise-Gondola shear zone (MGsz). The interaction of these shear zones with the Apennines chain is not yet clear. To address this open question we developed a set of scaled analogue experiments, aimed at analyzing: 1) how dextral strike-slip motion along a pre-existing zone of weakness within the foreland propagates toward the surface and affects the orogenic wedge; 2) the propagation of deformation as a function of displacement; 3) any insights on the active tectonics of Southern Italy. Our results stress the primary role played by these inherited structures when reactivated, and confirm that regional E-W dextral shear zones are a plausible way of explaining the seismotectonic setting of the external areas of the Southern Apennines.

1. Introduction

The active tectonics of the Italian peninsula is mainly characterized by a SW-NE oriented extension [*Montone et al.*, 2004], which occurs all along the axis of the Apennine chain (north of the Calabrian arc; Figures 1 and 2). In particular, along the topographic divide of the Southern Apennines this extension accounts for large earthquakes generated by NW-SE striking normal faults [*Gruppo di Lavoro CPTI*, 1999; *Boschi et al.*, 2000; *Galadini et al. eds.*, 2000; *Valensise and Pantosti eds.*, 2001, and references therein]. However, the 2002 Molise earthquakes (Figure 2), generated by E-W right-lateral faults located to the NE of the Southern Apennines, supplied living evidence that in this part of the chain, toward the foreland, NW-SE normal faulting gives way to E-W, right-lateral, seismogenic faults. These structures extend for tens of kilometers below the outer front of the Southern Apennine orogenic wedge (Figure 1) and, toward the east, below the foredeep deposits up to the foreland. Their present-day activity is suggested by both geological and seismological data, but their inception and growth date back to Mesozoic times. Therefore, their activity is interpreted as the reactivation of inherited zones of weakness.

Major E-W oriented shear zones have been singled out roughly between the latitudes 40°30'N and 42°30'N, both on-shore and off-shore [*Di Bucci and Mazzoli*, 2003; *Valensise et al.*, 2004, and references therein]. Among them, the best constrained runs through the source region of the 2002 Molise earthquakes, continues toward the east crossing the mesoseismal area of the 1627 Gargano earthquake, then connects with the Mattinata fault and the Gondola line off-shore (Figures 1 and 2). This shear zone, which we will refer to as Molise-Gondola shear zone (MGsz), can be considered as representative of all the other, generally less detailed, parallel shear zones.

The Mattinata fault, and more in general the E-W deformation belt between this structure and the Tremiti Islands (Figure 1), was considered as the expression of a change of thickness in the Adriatic lithosphere, thicker to the south with respect to its northern counterpart [*Calcagnile and Panza*, 1981; *Favali et al.*, 1993; *Doglioni et al.*, 1994]. From a geodynamic point of view, this deformation belt was interpreted as a right-lateral transfer zone accommodating higher roll-back velocities in the northern Adriatic slab with respect to the southern part [*Doglioni et al.*, 1994]. A more recent interpretation of all the active shear zones described above (i.e. from 40°30'N to 42°30'N) emphasizes the role of the Africa-Eurasia plates NW-SE convergence (well established, based on GPS an VLBI data: *DeMets et al.* [1990]; *Ward* [1994]; *Zarraoa et al.* [1994]; *Hollenstein et al.* [2003]; *McClusky et al.* [2003]) in controlling the seismotectonics of the Italian peninsula [*Di Bucci and Mazzoli*, 2003; *Valensise et al.*, 2004]. However, the interaction of these shear zones with the Apennine chain remains to be elucidated.

In this general perspective, we developed and analyzed a set of sandbox models, aimed at:

1) investigating how dextral strike-slip motion along a pre-existing zone of weakness within the foreland, both exposed at the surface and buried below the outer front of the orogenic wedge, propagates toward the surface and affects the wedge itself;
2) analyzing the propagation of deformation from this inherited structure as a function of displacement;
3) discussing any insights analogue modeling may supply on the active tectonics and seismogenesis along regional E-W shear zones, particularly in Southern Italy.

2. Geological setting

2.1. Regional setting

The Apennine fold-and-thrust belt of peninsular Italy (Figure 1) forms part of the Africa-verging mountain system in the Alpine-Mediterranean area. It is part of a Late Cenozoic accretionary wedge resulting from gravity-induced sinking of the Adriatic and Ionian Sea lithosphere and related subduction roll-back [e.g. *Patacca and Scandone,* 1989]. In the Southern Apennines, this wedge is formed by the orogenic stack of mainly east-to-northeast verging thrust sheets [see, e.g., *Mostardini and Merlini,* 1986], which derive from paleogeographic domains of alternating Meso-Cenozoic carbonate platforms and pelagic basins. The most external of these domains is represented by the Apulia Platform (Figure 1). Further to the east, a transition facies of this paleogeographic domain toward a pelagic basin is seen in the Gargano Promontory and in the Puglia off-shore, i.e., out of the chain. Deposits referred to both these marine paleodomains characterize the so-called Adriatic foreland.

The Apulia Platform (Table 1) consists of ~ 6 km thick, shallow-water, Mesozoic carbonates stratigraphically overlain by Upper Messinian and/or Pliocene evaporitic and terrigenous marine deposits [*Ricchetti et al.,* 1988; *Ciaranfi et al.,* 1988]. The deepest ~ 1000 m of this succession are made up of Triassic anhydrite-dolomite deposits [*Butler et al.,* 2004]. Very little is known about the deposits underlying the Apulia Platform succession, except that a few deep wells found fluvial-deltaic terrigenous facies of Permo-Triassic age [*Bosellini et al.,* 1993; *Butler et al.,* 2004]. Based on magnetic and gravimetric data, an igneous/metamorphic Paleozoic basement is hypothesized below these deposits [among others: *Mostardini and Merlini,* 1986; *Chiappini et al.,* 2000; *Tiberti et al.,* 2005].

The Apulia Platform and the underlying basement are partly involved in the orogenic wedge, partly form the foreland inflected below the outer front of the Apennine chain and related

foredeep deposits, and partly form the foreland *s.s.*, both on-shore (Gargano and Puglia) and off-shore (Southern Adriatic Sea; Figures 1 and 3) [*Mostardini and Merlini*, 1986; *Casero et al.*, 1988; 1991; *Doglioni et al.*, 1994; *Menardi Noguera and Rea*, 2000; *Patacca et al.*, 2000; *Morelli*, 2002; *Butler et al.*, 2004]. Southern Apennines thrusting and associated foredeep/thrust-top basin sedimentation progressed toward the Adriatic foreland up to the Middle Pleistocene within a SW-NE oriented contractional regime. Thrusts were often accompanied by normal and strike-slip faults; indeed the entire chain has been described as a paired tectonic belt with extension in the orogenic hinterland balancing orogenic contraction on the foreland-ward side of the orogen [e.g., *Lavecchia*, 1988].

The front of the orogenic wedge reached the present-day location and stopped at the beginning of the Middle Pleistocene [*Patacca and Scandone*, 2004b]. Indeed, a geodynamic change occurred around 800 ka, when a SW-NE extension became dominant over the core of the Apennines, as shown by geological and geomorphological analyses [*Cinque et al.*, 1993; *Galadini*, 1999; *D'Agostino et al.*, 2001]. It is worthwhile noting that Mt. Vulture, the only volcano within the Apennine chain, is Middle Pleistocene in age (oldest deposits dated 730 ka; *Beneduce and Giano* [1996] and references therein; Figure 1). This tectonic regime is still active, as demonstrated by breakout and seismicity data [*Montone et al.*, 1999; *Valensise and Pantosti eds.*, 2001]. As stated earlier, however, areas NE of the Apennine axis display a regime where a NW-SE horizontal compression accompanies a SW-NE striking σ_{hmin} [*Montone et al.*, 2004].

2.2. The Molise-Gondola shear zone (MGsz)

The E-W striking MGsz (Figure 1), roughly running at the latitude 41°40'N, can be traced for a total length of at least 180 km. Overall the system appears as a ~ 15 km-wide corridor from the Adriatic foreland off-shore to the core of the Apennines fold-and-thrust belt. Its off-shore portion is known as Gondola line [*De' Dominicis and Mazzoldi*, 1987; *Colantoni et al.*, 1990; *de Alteriis*, 1995; *Morelli*, 2002; Figure 1]. This line affects the sea bottom, suggesting Quaternary activity, but seismic reflection lines allowed its motion to be detected since Cretaceous [*Aiello and de Alteriis*, 1991; *Argnani et al.*, 1993; *de Alteriis*, 1995; *Morelli*, 2002; *Patacca and Scandone*, 2004a]. Therefore, this line has been repeatedly reactivated by different tectonic regimes before, during and after the Apennine chain build-up (e.g., Mesozoic extension or Cenozoic shortening), both with right- and left-lateral components of motion.

Moving westward, the Gondola line comes ashore in the Gargano Promontory as Mattinata fault (Figure 1). This important structure of the Adriatic foreland has been intensely investigated from a regional, structural and seismotectonic point of view [*Finetti*, 1982; *Funiciello et al.*, 1988;

Winter and Tapponier, 1991; *Billi and Salvini*, 2000; *Chilovi et al.*, 2000; *Billi*, 2003; *Piccardi*, 1998; *Borre et al.*, 2003]. Also in this case, a polyphase activity has been recognized, and the complex fault kinematics is still matter of debate. Nevertheless, most investigators agree on a present-day right-lateral main component of motion, as confirmed by the focal mechanisms of the 19 June 1975 and 24 July 2003 earthquakes (Figure 2), GPS data [*Anzidei et al.*, 1996; *Ferranti and Oldow*, 2005], geomorphological and paleoseismological investigations [*Piccardi*, 1998; *Borre et al.*, 2003; *Piccardi*, 2005]. Indeed, the Mattinata fault has already been interpreted as the source of historical earthquakes (e.g.: 493 AD, 1875), and instrumental seismicity is normally recorded within the first 25 km of the crust of the Gargano area [*Piccardi*, 1998; *Valensise and Pantosti eds.*, 2001; *Valensise et al.*, 2004; *Castello et al.*, 2005].

Further to the west, the foreland plunges with a dip angle of ~ 10° below the Plio-Pleistocene deposits filling the Bradanic Trough, i.e. the most recent foredeep [*Mariotti and Doglioni*, 2000; Figures 1 and 3]. However at depth, at the top of the buried Apulia Platform, an E-W ridge is preserved along strike of the Mattinata fault. This structure, known as Chieuti high (Figure 1), has been interpreted as a horst [*Casnedi and Moruzzi*, 1978] and, more recently, as a push-up related to strike-slip motion [*Patacca and Scandone*, 2004a]. It is accompanied by WNW-ESE striking, SSW dipping faults with a normal component of motion, one of which (the Apricena fault, to the north of the Chieuti high) has been interpreted by *Patacca and Scandone* [2004a] (Figures 1 and 2) as the seismogenic source of the 1627 Gargano earthquake (Me = 6.8; *Gruppo di Lavoro CPTI* [1999]). Scattered clues of recent activity on E-W structures, both in this area and more to the west, are also provided by the drainage pattern, that shows consistent E-W trending anomalies [*Valensise et al.*, 2004].

Finally, the Apulia Platform and underlying basement deepen below the outer front of the Apennine orogenic wedge, where the 2002 Molise earthquakes occurred (Figures 1 and 2). Both the mainshocks of the sequence had similar magnitude (Mw = 5.8-5.7), hypocenters at 16 and 18 km, respectively [*Vallée and Di Luccio*, 2005], and almost pure strike-slip focal mechanism, with right-lateral motion on E-W trending nodal planes (Figure 2). The aftershocks distribution also follows an E-W direction, and surface coseismic deformation revealed by GPS data is consistent with this kinematics [*Giuliani et al.*, 2003], but no surface faulting accompanied these earthquakes. Activity mainly took place in a crustal volume extending between 10 and 24 km depth [*Valensise et al.*, 2004]. In this area, the buried Apulia Platform is ~ 6 km thick and its top lies at ~ 3000 m depth [*Mostardini and Merlini*, 1986]; this implies that the seismogenic structures of the 2002 Molise earthquakes are located essentially within the Paleozoic basement of the Apulia Platform.

Whether and how the MGsz continues toward the west is not known. A possible interpretative key is provided by the 1990 Potenza seismic sequence, that occurred on a parallel shear zone located more to the south (40°30'N latitude; Figures 1 and 2). The focal mechanism of the 1990 mainshock exhibits right-lateral slip on an E-W striking plane, and the aftershocks distribution is roughly elongated in the same direction, with the hypocenters mostly concentrated between 14 and 25 km [*Azzara et al.*, 1993; *Demanet et al.*, 1998; *Di Luccio et al.*, 2005b]. Projecting these data onto a geological cross section at regional scale [e.g., *Menardi Noguera and Rea*, 2000; *Butler et al.*, 2004], one can observe that also the 1990 Potenza sequence occurred within the basement underlying the Apulia Platform (Figure 3). Moreover, this sequence was generated within the most internal buried foreland, where it tends to deepen below the outer front of the Apulia antiformal stack (i.e., the deepest part of the Apennine chain). This means that right-lateral E-W striking shear zones could be active at least as far as the buried Adriatic foreland is not involved in thrusting. Tentatively, one can hypothesize the same behavior also for the MGsz, that may thus extend for at least 10-15 km west of the 2002 Molise earthquakes epicentral zone [*Mostardini and Merlini*, 1986; *Butler et al.*, 2004].

With respect to the Apennine chain, the foreland buried below the outer front of the Apulia antiformal stack is the most internal structural domain where active tectonics and seismicity are known to occur along E-W striking shear zones. Indeed, along the axis of the Apennine belt strong earthquakes on NW-SE normal faults are the expression of active extension characterized by a SW-NE-oriented σ_3. This seismicity is generated by faulting within the uppermost 15 km of the crust [*Valensise e al.*, 2004], and is best represented by the 1980 Irpinia earthquake (Ms = 6.9; *Gruppo di Lavoro CPTI* [1999]), that nucleated at about 13 km depth [*Boschi et al.*, 1993] (see Figures 2 and 3 for its focal mechanism and location). It is still not clear whether shallow extension along the Apennine axis may coexist and be compatible with a different stress field at deeper crustal levels, such as that affecting the external areas where NW-SE compression accompanies a SW-NE striking extension. Therefore, hypotheses about a possible continuation of the MGsz to the west, below the Apennine axis and where the Adriatic foreland is disrupted by thrusting, still remains speculative and in need of further investigations.

Finally, it has to be noted that large discrepancies can be found in the literature about the displacement along the MGsz, also depending on the considered lapse of time and on the sense of motion. For the Meso-Cenozoic activity, the maximum displacement referred to dextral strike-slip motion is of about 15 km [*De' Dominicis and Mazzoldi*, 1987], while the only available estimate for the left-lateral motion, based on pull-apart geometries and considered as a minimum, is 2-3 km [*Billi*, 2003; *Billi*, pers. comm.].

For the right-lateral displacement related to the most recent activity of the Mattinata fault, *Chilovi et al.* [2000] suggest it started in Upper Pliocene times, and refer to the Upper Pliocene-present the displacement of 15 km detected by *De' Dominicis and Mazzoldi* [1987], implying a horizontal slip rate of about 6 mm/a. For the Upper Pleistocene-Holocene, *Piccardi* [1998] proposes a vertical slip rate of 0.7 +/- 0.2 mm/a and a horizontal slip rate of 1.0 +/- 0.2 mm/a. Assuming the present-day tectonic regime as acting since the Middle Pleistocene and the horizontal slip rate as constant during this lapse of time, we obtain a total displacement ≤ 1 km. Being inactive since Middle Pleistocene, the front of the Southern Apennines could be a useful benchmark for estimating the displacement that has taken place since that time along the MGsz. Unfortunately this front is buried under part of the Bradanic foredeep deposits and sealed by them (Figure 1). Therefore, the location of the outer front of the Southern Apennines is not sufficiently constrained for our purposes.

Summing up, cumulative horizontal displacement referred to the active tectonic regime ranges between 1 and 15 km.

3. Experimental set-up

Sandbox models are a simplified reproduction of the crustal volume formed by the foreland hosting the MGsz and by the overlying yet inactive outer front of the Apennine orogenic wedge (Plio-Pleistocene foredeep deposits included). The models were scaled at 1:200,000, as described in Table 2, where models' dimensions are shown in comparison with the corresponding geological data. They were scaled to natural dimensions by observing geometric, kinematic and dynamic similarity relationships [*Hubbert*, 1937; *Ramberg*, 1981]. We assumed that 0.5 cm in the models corresponds to 1 km in nature.

Then,

$C_p/\rho_p = 5 \times 10^6 \, C_m/\rho_m$

where subscript *p* denotes natural conditions, subscript *m* analogue model conditions, *C* is cohesion and ρ is density. Using an average density of ρ_m = 1500 kgm^{-3} and ρ_p = 2800 kgm^{-3}, cohesion of 10 Pa in the model corresponds to ~ 100 MPa in nature.

The angles of internal friction (ϕ) are equal at both scales. In particular, two types of granular materials were used with different physical parameters: sand and glass microbeads. The sand has ϕ = 33° and a grain size of 100–300 μm. Glass microbeads are suitable for simulating natural rocks because they enable low basal friction detachment [*Sassi et al.*, 1993] and inter-strata slip [*Turrini et al.*, 2001] to occur. Glass microbeads have ϕ = 24°, due to their high sphericity and rounding [*Schellart*, 2000], and a grain size of 300–400 μm. The basal detachment has ϕ = 32°.

The experimental apparatus (Figure 4) was provided with a baseplate fault, which extended for the whole length of the models and accommodated a right-lateral simple shear. The basal displacement varied for each model.

Five models were realized. The first model (SS02, Table 3) was prepared to reproduce a typical wrench zone as classically described in literature (among many others: *Wilcox et al.* [1973]; *Christie-Blick and Biddle* [1985]; *Harding* [1985]; *Naylor et al.* [1986]; *Sylvester* [1988]; *Richard and Cobbold* [1990]; *Richard et al.* [1995]; *Mandl* [2000]; *Nieuwland and Nijman* [2001]). It has a constant thickness of 10 cm and no discontinuity of any sort within the sand volume (neither layers of glass microbeads, nor cuts). The displacement applied on the baseplate fault was of 8.0 cm. This model was used as a reference for four additional models (SS03 to SS06, Table 3), all specifically designed for the present study.

These four models are characterized by a layer of glass microbeads within the foreland, aimed at simulating Triassic evaporites (see Table 1), and at the interface between buried foreland and wedge (Figure 4). The foreland-side of the models (included the part below the wedge) has a vertical discontinuity perpendicular to the wedge front obtained through a cut that reorganizes the grain distribution [*Sassi et al.*, 1993; *Viola et al.*, 2004], whereas no discontinuity exists in the chain-side and in the wedge itself (Figure 4). The baseplate fault of the experimental apparatus coincides with the discontinuity in the foreland-side. The chain-side is also characterized by a slightly larger thickness to account for topography (Tables 2 and 3).

The displacement on the baseplate fault was progressively larger in these four models: 0.5, 3.0, 5.5 and 8.0 cm (Table 3), with the minimum and maximum values coming from the literature (Table 2) and the other two chosen as intermediate steps.

Summing up, the experimental set-up was intended to identify three regional-scale domains, east to west (Figure 4):

- domain **A** - the foreland, corresponding to the Adriatic foreland;
- domain **B** - the wedge; it corresponds to the outer front of the Apennines orogenic wedge (including the most recent foredeep) and to the underlying buried foreland;
- domain **C** - the chain, corresponding to the core of the Apennine fold-and-thrust belt.

In the following we will refer to these domains simply as **A**, **B**, **C**.

4. Experimental results

All the experiments were monitored with map-view pictures taken at every 0.5 cm step of basal displacement. As the models' geometries are the result of known and imposed kinematics, we

will first describe the kinematics, then show the resulting geometries. The deformation kinematics of the reference model SS02 (Figure 5a-h) is compared to model SS03 (Figure 5i-s), which has the same final displacement of 8.0 cm and includes all the deformation steps of the other experiments. The resulting geometries are then shown starting from the least deformed model. We present only few key sections for each experiment, although the interpretation rests on the whole dataset, based on 2 cm-spaced sections cut perpendicular to the baseplate fault. When reported, fault strike is measured clockwise with respect to the baseplate fault; negative values imply a counterclockwise measure.

4.1. Deformation kinematics

4.1.1. Deformation kinematics - model SS02 (constant thickness and no discontinuity of any sort within the sand volume; total displacement: 8.0 cm)

After 0.5 cm of basal displacement the first fault formed in the western open side of the apparatus, whereas only smooth grid deformation occurred all along the surface of the model (Figure 5b). Other faults striking 20° to 28° developed after 1.5 cm of displacement (Figure 5c). They can be interpreted as synthetic Riedel faults that developed near the baseplate fault at the two open sides of the box. They also propagated at their tips forming high-angle splays (from 35° to 40°).

After 2.0 cm of displacement (Figure 5d), a second group of faults formed, with strike ranging from 13° to 22°.

A swarm of faults appeared diffusely on the entire surface of the model at D = 3.0 cm (Figure 5e); they were organized *en échelon* and left-stepped, consistent with the dextral shearing. In general, faults formed astride the baseplate fault and propagated on both sides. The maximum displacement occurred in the middle, terminating toward the fault tips.

At D = 4.5 cm, synthetic low-angle faults (from -4° to 6°) appeared for the first time, sub-parallel to the baseplate fault (Figure 5f). Then P faults developed (from -12° to -7°) between Riedel faults, without cutting them. At the same time, the external branches of the Riedel faults deactivated. The formation of P shears *sensu Tchalenko* [1970] generated a characteristic rhomboidal fault pattern.

In the following step (D = 5.5 cm; Figure 5g), only the faults closest and sub-parallel to the baseplate fault were active.

No new faults formed in the final 2.5 cm of basal displacement (Figure 5h), the deformation being almost completely accommodated by the same faults. This implies that the deformation kinematics achieved a steady-state for a displacement of ca. 5.5 cm. This value corresponds to about

a model half-thickness; however, the possible relationship between steady-state achievement and model thickness is in need of further analyses that are out of the scope of this work.

4.1.2. Deformation kinematics - model SS03 (variable thickness, stratigraphic and tectonic discontinuities within the sand volume; total displacement: 8.0 cm)

In this model, the applied displacement was immediately transferred to the pre-existing cut in the foreland domain **A** up to the model surface (Figure 5m, fault P). The deformation propagated toward the west through the wedge front (domain **B**) and the first rectilinear dextral fault started to form. Grid lines were distorted almost everywhere.

After D = 1.5 cm (Figure 5n) several dextral faults appeared. Faults #2 and #4 branched from the fault P with a curved shape. Both extended in the receding side of the model only, with maximum strikes of 23° and 27°, respectively. Toward the western open side of the model, faults #3 and #5 formed with sinusoidal shape, their strike increasing at their tips.

At D = 2.0 cm (Figure 5o), a new fault (#6) propagated from the P fault and continued in the chain domain **C**, with strike similar to the previous faults. At the same time, faults #2 and #4 were almost deactivated. Synthetic Riedel faults formed as well (#7 and #8) with strikes ranging from 16° to 19°.

After D = 3.0 cm (Figure 5p), faults #6 and #8 went on move.

At D = 4.5 cm, fault #10 branched from fault #6 with a curved shape. At the same time, three faults formed (#11, #12 and #13, Figure 5q) close to the surface projection of the baseplate fault, arranged slightly *en échelon*. They were low-angle faults with strikes ranging from –1° to –5°. Subsequently, they joined one another and with fault P (D = 5.5, Figure 5r). At this step, fault #8 deactivated whereas fault #10 went on move, but very slowly.

No new faults were observed during the following steps toward the end of the experiment (D = 8.0 cm, Figure 5s) and almost all the deformation was accommodated by the longest E-W fault in the middle of the model. Also in this case the deformation kinematics achieved a steady-state for a displacement corresponding to about 5.5 cm.

4.2. Deformation geometries

4.2.1. Deformation geometries - model SS06 (total displacement: 0.5 cm)

The final displacement for this model was D = 0.5 cm (compare the map-view of Figure 6 with Figure 5m and n). In map-view, in the foreland domain **A** the imposed basal displacement was accommodated exclusively by the pre-existing discontinuity P. Fault P offset the wedge front and propagated into domain **B** with a clear bend-off towards the receding half, as expected from the

stress change induced at the tip of a strike-slip fault (*Mandl* [2000], *Lopes Cardozo et al.* [2002], *Kim et al.* [2004]; also see the subsection 5.2. in the Discussion). We will recognize this style in domain **B** of all models. In this case, two faults partitioned the deformation and formed a restraining stepover. At surface, fault #1 is 8.0 cm long and shows a displacement of 3 mm, whereas fault #2 is 6.3 cm long. Toward the chain, the distorted grid lines were the only evidence of diffuse deformation.

In cross section, the location of fault planes was largely inferred as the layers do not appear clearly displaced and the faults seemed to accommodate only strike-slip activity. Only the contemporaneous view of the surface and the interpretation of the entire set of sections of all models allowed these subtle faults to be detected. Sections cut in the wedge domain **B** showed that both fault splays #1 and #2 branched at the upper tip of the pre-existing fault P. They became deeper and less inclined as the P tip deepens (from 2 cm depth and 76° in section 58, to 8 cm depth and 56° in section 44). At this step of deformation, the vertical throw is either unresolvable or does not exist at all.

4.2.2. Deformation geometries - model SS05 (total displacement: 3.0 cm)

The final displacement for this model was D = 3.0 cm (compare the map-view of Figure 7 with Figure 5p). At the end of the experiment, faults P, #7 and #8 were active. In map-view, the fault pattern was much more complicated with respect to the previous step. In the foreland domain **A**, displacement was exclusively accommodated by fault P. Within the wedge domain **B**, four synthetic faults (#1, #3, #5 and #8) affected the receding half of the model. The length of their surface trace increased from 10 to 27 cm, with a maximum strike-slip displacement of ~ 1 cm, close to the baseplate fault projection. In the chain domain **C**, five faults were present astride the baseplate fault. Fault #7 reached 1 cm of dextral offset. At the surface, the deformation belt as a whole showed a maximum width of about 20 cm. Also at depth (s66) the reactivated discontinuity P was the only detectable structure in domain **A** and accommodated the displacement without any vertical throw. In domain **B**, all the faults rooted close to the upper tip of the fault P. The fault pattern (#1, #3, #5 and #8) formed asymmetric flower structures, with both reverse and normal vertical throw. For example, fault #1 in section 54 showed a normal throw of ~ 1 mm and a horizontal slip of ~ 3 mm. Along strike, fault #1 no longer reached the surface and was finally replaced by faults #3 and #5 (s48). At depth (s42), fault #3 showed a subtle vertical throw; along strike this fault becomes blind, and a change in the vertical throw also occurs, from normal to reverse (s38). In all models, the normal component of motion is seen only in the deeper portion of the fault planes in domain **B**. This may be a direct consequence of the propagation of the buried pre-

existing discontinuity through the overlying wedge deposits. Also in this case this behavior may be explained by the stress change induced at the tip of a strike-slip fault [*Mandl*, 2000; *Lopes Cardozo et al.*, 2002; *Kim et al.*, 2004], where an extensional stress field occurs in the receding block. Toward the west, in the chain domain **C**, faults rooted in the baseplate fault and had reverse displacement. They formed a typical symmetric flower structure (s26), resulting in nearly 0.5 cm of topographic uplift.

4.2.3. Deformation geometries - model SS04 (total displacement: 5.5 cm)

The final displacement was D = 5.5 cm (compare the map-view of Figure 8 with Figure 5r). At the end of the experiment, the active structures were faults P, #12 and partially #9. Their linkage finally resulted in a continuous dextral strike-slip fault that separated completely the two halves of the model. At the surface, the deformation belt as a whole showed a maximum width of about 15 cm and ~ 0.8 cm of topographic uplift. Again, in the wedge domain **B** the fault pattern was asymmetrical and developed only in the northern block, and all the faults branched at the upper tip of the buried pre-existing cut. Along strike, faults terminated upwards (s50, fault #1), therefore only part of the fault planes reached the surface. Moreover, at this stage of the model evolution, truly blind faults seemed to occur locally (s26, s36 and s38, faults **a** and **b**), without clear evidence at shallower levels. The normal component of throw was quite evident for all faults, but was more developed in the high-angle faults (#3 and #5, s48-s38). In the chain domain **C**, faults developed as symmetric flower structures branching from the baseplate fault.

4.2.4. Deformation geometries - model SS03 (total displacement: 8.0 cm)

The final displacement was D = 8.0 cm (Figures 5 and 10). The fault pattern was similar to that of the previous model (SS04, Figure 8). Actually, no new faults formed during the final 2.5 cm of basal displacement, and the continuous E-W fault formed by the linkage of faults P, #11, #12 and #13 accommodated the whole deformation. Only fault #10 remained partially active (Figures 5r and s, and 9). At the surface, the deformation belt as a whole showed a maximum width of about 14 cm. Topographic uplift exceeded 1.0 cm in domain **C** (s26).

5. Discussion

The results of our study define the pattern of newly formed faults as being strongly controlled by the pre-existing discontinuity, which influenced the location and geometry of the new fault planes as well as the kinematics of the entire shear zone and the way deformation is

partitioned. On the contrary, no significant effects resulted from the presence of layers of glass microbeads. All these topics will be discussed in detail in the following subsections in comparison with the reference model.

5.1. The "reference model" kinematics

The kinematics of model SS02 (the reference experiment, Figure 5a-h) is very close to that of published experiments with similar initial conditions [*Naylor et al.*, 1986; *Mandl*, 1988, 2000; *Richard and Cobbold*, 1990; *Richard et al.*, 1995; *Ueta et al.*, 2000; *Nieuwland and Nijman*, 2001; *Viola et al.*, 2004], i.e. overburden wrench faulting in basement-controlled models. After few displacement steps, deformation takes place diffusely at the surface of the model. Grid lines bend for a width of about 12-15 cm after D = 2.5 cm, and then faults grow inside the area.

It is important to notice the influence of the open sides of the box, which mainly depends on the thickness of the sand tapering to zero toward them. These open sides, and particularly the western one, affect the development of Riedel faults that form in the early stages of displacement. There, faults seem to form with strike greater than usual and after less steps of displacement. As a matter of fact, faults occur first close to the open side of the apparatus (after 0.5-1.0 cm of basal displacement) and then in the center. The greatest development of Riedel faults in the middle of the model starts between 2.0 and 3.0 cm of displacement.

5.2. Pre-existing discontinuity: effects on the kinematics

The pre-existing cut in models SS03 to SS06 strongly modified the deformation kinematics with respect to model SS02 (also see *Richard and Krantz* [1991]). It always worked as a preferential slip surface in the foreland domain **A**, thus accommodating the basal displacement since the very first stages of deformation and preventing the inception of any new structures. Even if displaced during the deformation, the grid lines indeed remained perfectly straight on the two sides of the fault. The presence of the layer of glass microbeads within the sand had no effects, regardless of the amount of displacement.

Toward the wedge domain **B**, the motion on the pre-existing cut propagated only in the receding (i.e. northern) block, producing distortion of the grid lines, precursor of the development of faults. This behavior, well known in the literature [*Mandl*, 1988; *Lopes Cardozo et al.*, 2002] is determined by the pre-existing fault itself, that causes perturbation of the stress field in the tip regions. This is because the fault is characterized by a lower Young modulus and a lower shear strength than the adjacent materials, limiting the shear stress carried by the fault. As a consequence, a deflection of the σ_1 trajectories occurs near the leading edge of the fault. Qualitatively, this can be

easily understood, since the material is compressed on the advancing side of the fault (where the domain **A** acted as a buttress for the adjacent domain **B**) and stretched on the receding side [*Mandl,* 2000]. The developing faults are synthetic *en échelon* faults which form in a sequence from east to west. Normally, the formation of a new fault coincides with the deactivation of the former one. In general, it appears that the propagation of deformation took place from the foreland domain **A** to the chain domain **C** through the wedge domain **B**. In practice, deformation was transferred from fault P to the faults in the wedge domain **B** and finally to the low angle faults in the chain domain **A**. To the south of the fault P, grid lines remained almost undeformed, suggesting a partial inactivity similar to what happened in the foreland area.

In section 4 (Experimental results) we observed that the deformation kinematics achieved a steady-state for a displacement of ~ 5.5 cm. This state is characterized by (i) an essentially continuous activity of the faults near parallel to the E-W baseplate-fault; (ii) the deactivation of minor faults striking at high angles with respect to the baseplate fault; (iii) the lack of inception of new faults. These main traits fit with the steady-state as described by *Tchalenko* [1970]: “Nearly all displacement takes place along a single principal displacement shear superimposed on the interface between the two half of the model. The shearing resistance is stable and at its residual value”.

In cross section, faults seem to propagate upward from the baseplate fault in the chain domain **C**, whereas they branch from the upper tip of the pre-existing fault in the wedge domain **B**. As a matter of fact, the buried pre-existing cut acts as an effective baseplate fault just below the wedge. The immediate activation of the cut furthers an early inception of faults in the northern half of domain **B** (compare kinematics in Figure 5).

5.3. Geometry of structures

The length and spacing of the faults, the width of the shear zone and the timing of development are all known to be mainly related to the thickness of the sand pack [*Tchalenko,* 1970; *Naylor et al.,* 1986; *Mandl,* 1988, 2000; *Richard et al.,* 1995; *Schöpfer and Steyrer,* 2001]. In the northern side of the wedge domain **B**, length and spacing of the faults increase to the west, as well as their vertical extent. An inspection of the vertical sections makes it clear that the depth of the pre-existing cut controls the faults geometry. From east to west, the thickness of the foreland affected by the pre-cut diminishes whereas the overburden chain increases. This means that the influence of the pre-cut diminishes toward the chain together with the foreland thickness. The buried pre-cut works as an effective baseplate fault for the overlying wedge as it directly transmits the slip from the base upward. Accordingly, the shear zone width measured at the surface increases toward the west as the overburden sand pack increases (compare domains **B** and **C** in Figure 5q-s).

Blind faults appear in all models, but they are not always truly blind. As the lateral view of a Riedel fault plane has a parallelogram shape, the lateral terminations are not vertical and the tip lines are three-dimensional [see *Naylor et al.*, 1986, Figure 6]. Hence, in some sections, faults terminate upwards or downwards. In this perspective, such faults are only locally blind. Strictly blind faults, i.e. faults that never affect the surface of the models, seem to appear only in model SS04 (labeled as **a** and **b** in Figure 8: s26, s36 and s38).

5.4. Deformation partitioning

The pre-existing discontinuity strongly modifies the normal deformation partitioning (Figure 5). In foreland domain **A**, all visible deformation is accommodated by this fault. Grid lines remain undeformed and also a close inspection of the model surface does not reveal subsidiary structures nearby. The attitude of the pre-cut surface with respect to the baseplate fault and its lower frictional resistance allow its complete and prompt activation. In this domain, topography remains almost unchanged, as no vertical movement occurs. In the wedge domain **B**, faults start to form after a few millimeters of basal displacement and cease to grow at D = 3.0-4.0 cm (Figure 5p). Subsequently, the deformation is transferred to new structures toward the chain domain **C**.

The deformation on the faults is quite complex and it has been sketched in Figure 10. In map-view, the fault branches from the main dextral wrench fault in the middle of the model. It shows a curved shape: in its initial part (Figure 10, sX), fault is sub-parallel to the main fault and accommodates a great horizontal offset. In section, it is steeply dipping, has a shallow depth, a small normal throw and thus is slightly transtensional. Along strike, fault diverges more from the main fault, decreasing the horizontal offset. In section, it deepens while the dip angle decreases. In particular, it changes the vertical throw from normal at depth to reverse near the surface. Toward its termination, a transpressive kinematics characterizes the entire width of the fault, with similar vertical and horizontal components of displacement (Figure 10, sZ). Such attributes imply a scissor kinematics on the fault plane, i.e. a block rotation about a sub-horizontal axis. As a matter of fact, Riedel shears developed with a helicoidal surface, i.e., their attitude changed continuously both vertically and horizontally. This resulted from the re-orientation of the principal stress axes, as the shear stress decreases at the same time both along the fault strike, away from the pre-existing fault, and along the fault dip, from the pre-existing fault toward the surface. As a consequence, where faults dip gently, strike-slip deformation is also accommodated with a slightly compressional secondary component; where faults dip steep, the secondary component is instead extensional [*Naylor et al*., 1986; *Mandl*, 1988; *Nieuwland and Nijman*, 2001].

Topography is practically unchanged in the block unaffected by faults, whereas in the other block smooth vertical movements affect the surface.

In the chain domain **C**, where there is no pre-existing discontinuity, the baseplate fault controls completely the structural style of the overburden. The shear zone attains its maximum width in parallel with the maximum thickness of the overlying sand pack [*Tchalenko,* 1970; *Schöpfer and Steyrer,* 2001]. Grid lines start to be greatly deformed long before faults reach the surface. Transpression occurs principally in the chain domain **C** and results in the highest topographic relief. The reverse vertical throw is greatest at the surface and vanishes with depth, where mostly pure strike-slip occurs.

6. Insights on the active tectonics and seismicity pattern in Southern Apennines

The integration of the results of this work with information available in literature allows us to (i) provide an interpretative key for specific characteristics of the MGsz not previously addressed (Figure 11), and (ii) discuss the insights supplied by analogue modeling on the active tectonics along regional E-W shear zones, particularly in Southern Italy.

Our first piece of evidence concerns the present-day tectonic activity of the Mattinata fault (Figure 1). The chances that this structure is fully reactivated up to the surface [*Piccardi*, 1998; *Borre et al.*, 2003; *Piccardi*, 2005] are confirmed by the analogue models also for extremely reduced displacement values (Figures 5m, 6 and 11). This full reactivation inhibits the inception of any other fault, suggesting the absence of newly formed active ancillary structures associated with the Mattinata fault, whatever their real displacement. This topic may form the object of future investigations.

Our second point deals with the Apricena fault (Figure 1). Based on the architecture of deposits seen in reflection seismic lines and well logs focused on the uppermost 4 km of the crust, this fault was hypothesized as the source of the 1627 Gargano earthquake by *Patacca and Scandone* [2004a] (Figures 1, 2 and 11). According to these investigators, the Apricena fault is a 30 km long, N286° striking, SSW dipping normal fault, cutting the whole Quaternary sequence in response to NW-SE large-scale extension. They interpret it as a primary structure under the current stress regime, whereas dextral strike-slip faults such as the Mattinata fault or the sources of the 2002 Molise earthquakes are considered as transfers between large normal faults, that is to say, secondary structures. Finally, they describe the faults bounding the Chieuti high (Figure 1 and 11) as sealed by late Early Pleistocene deposits and therefore inactive.

Our experiments suggest an alternative and substantially different explanation. We think the Apricena fault could be interpreted as one of the splay faults developing at the front of the orogenic

wedge from the deeper, pre-existing discontinuity in domain **B** of our models. Recall that these splays (e.g., fault #1 in models SS06 and SS05; Figures 6, 7 and 11) are N288° striking, SSW dipping and exhibit a normal component of slip, and form also for relatively low displacements. Moreover, where these splays start deflecting from the direction of the shear zone, no structures are seen at shallow depth above the deep discontinuity (Figures 5n, 5o and 6). This would explain the state of inactivity of the faults bounding the Chieuti high, as proposed by *Patacca and Scandone* [2004a].

In summary, the geometry and kinematics of the Apricena fault are fully compatible with the hypothesis of it playing a subsidiary role with respect to the MGsz, which is instead the primary structure. This is especially true considering that seismic reflection lines rarely allow the horizontal component of displacement to be properly detected, and hence this fault may well have an unresolved strike-slip component of motion.

Our third point concerns the faults responsible for the 2002 Molise earthquakes (Figures 1 and 2). These are steeply dipping, right-lateral strike-slip faults, with a cumulative length of about 15 km, and extend from ca. 20 to 6 km depth without reaching the surface [*Vallée and Di Luccio*, 2005]. As recalled earlier, GPS data revealed coseismic deformation consistent with dextral kinematics [*Giuliani et al.*, 2003]. Despite the depth of the seismogenic faults, in the long run strain propagation must ultimately affect the topographic surface and generate the geomorphic and drainage network anomalies outlined by *Valensise et al.* [2004].

Experiments show that in the portion of domain **B** that corresponds to the structural setting of the 2002 Molise earthquakes (roughly corresponding to the section s48-s54 of the different models), the pre-existing strike-slip fault does not reach directly the models' surface until displacement exceeds ca. 5 cm, corresponding to ~ 10 km in nature (Figures 5q, 5r, 7, 8). However, also in case of smaller displacements the models' surface is affected by a ribbon of diffuse strain, both horizontal and vertical (Figure 6, s48), and in some cases by few oblique faults that diverge from the vertical projection of the E-W fault (Figure 7, s48). At the same time, partially blind faults affect this part of the models at moderate depth.

Considering the three points described above from a more general perspective, the comparison between our models and the structural setting of the study area further highlights that the complex fault pattern developed for high displacements does not find an obvious equivalent in the modeled part of the Apennines. This observation favors the hypothesis that the most recent and present-day activity of the MGsz has not yet accumulated a significant displacement. In particular, the relatively good fit between model SS06, part of SS05 and the real world suggests that cumulative displacements on the portion of the MGsz that lies between the Mattinata fault and the

2002 Molise earthquakes sources should fall in the 1-6 km range, but more likely closer to the lower bound. This corresponds to a slip rate value quite close to 1.3 mm/a, assuming the present-day tectonic regime as acting since the Middle Pleistocene. Conversely, our results allow displacements in the order of 10-15 km to be positively ruled out for the most recent phase of activity of the MGsz.

Finally, we can use our results and reasoning to speculate on the style of possible active structures west of the 2002 Molise earthquakes source area. To do that we move further toward the interior of the Apennine chain, in a structural setting comparable to that of the 1990 Potenza seismic sequence (see section 2.2. of the Geological Setting and Figure 3; it roughly corresponds to the section s38-s48 of the different models) and consider displacement values such as those discussed above (Figures 1, 2 and 11). Figures 6, 7 and 11 show that the right-lateral, deep vertical fault is accompanied by moderately- to steeply-dipping oblique faults, that in this part of the model may or may not reach surface depending on the horizontal offset. For instance, no surface faulting occurs for horizontal displacement values corresponding to ~ 1 km in nature (Figure 6). In any case, only surface faults directly connected to the deep fault are active with low displacement values (see Figure 5o and p).

7. Final remarks and conclusions

The analogue modeling has outlined the primary role played by E-W striking, inherited right-lateral faults in the foreland and at the front of a fold-and-thrust belt, when these structures are reactivated.

From a geodynamic point of view and referring to the Italian peninsula, the simple shear adopted in our modeling simulates the observed right-lateral kinematics, but does not provide constraints about the “engine” for the MGsz and the other parallel shear zones. However, geological and seismological evidence suggests that these shear zones affect large part of the external zones of the Southern Apennines, from the latitude 40°30’N to the latitude 42°30’N and perhaps beyond these bounds (Figure 1). This is a much wider area than the Tremiti-Mattinata deformation belt, which corresponds to the change of thickness of the Adriatic lithosphere and was interpreted as a right-lateral transfer zone, accommodating different roll-back velocities of the Adriatic slab [*Doglioni et al.*, 1994]. In our opinion, the coupling of NW-SE convergence of the Africa and Eurasia plates with pre-existing E-W discontinuities provides a reliable framework for understanding the active tectonics and the seismicity of the entire study region.

Although it is known from the literature that structures such as the MGsz can be best modeled with a simple shear (for instance, see *Sylvester* [1988]), we stress that this mechanism, the baseplate fault and the models presented here are obviously and necessarily simplified. The external areas of the Apennines are known to be affected by a stress field where a NW-SE compression accompanies a SW-NE striking extension. Variations in the value of the angle between the shear zones and the direction of compression can change the expected geometry and kinematics of the newly formed faults and reduce the applicability of the models. Moreover, real shear zones are not so rectilinear as in the models. This implies that transpressional or transtensional complexities unpredicted by the models may exist in the real geological case. Furthermore, given the geological nature of the different pre-existing E-W discontinuities, one can expect a certain variability in their length, width and strike. For instance, clues of E-W active features are available on-shore and off-shore for the MGsz and at the latitude of the Tremiti Islands [*Favali et al.*, 1993; *Del Monte et al.*, 1996; Figure 1], whereas similar features have never been recognized off-shore more to the south, between the MGsz and the latitude of Potenza [*Morelli*, 2002, and references therein]. Nevertheless, the experiments described provide an independent and innovative tool for addressing an important outstanding issue in Italian active tectonics, and confirm that regional E-W trending, dextral shear zones can play a fundamental albeit “hidden” role in the seismotectonic setting of Southern Italy.

Acknowledgments

We are grateful to R. Basili and P. Burrato for the useful discussions. Reviews by T. Winter and H. Koyi are also acknowledged. Work financially supported by INGV and by PRIN 2004 grant (University of Pavia).

References

Aiello, G., and G. De Alteriis (1991), Il margine Adriatico della Puglia: fisiografia ed evoluzione terziaria, *Mem. Soc. Geol. It., 47,* 197-212.

Anzidei, M., P. Baldi, G. Casula, M. Crespi, and F. Riguzzi (1996), Repeated GPS survey across the Ionian Sea: evidence of crustal deformations, *Geophys. J. Int., 127,* 257-267.

Argnani, A., P. Favali, F. Frugoni, M. Gasperini, M. Ligi, M. Marani, G. Mattietti, and G. Mele (1993), Foreland deformational pattern in the Southern Adriatic Sea, *Annali di Geofisica, 36 (2),* 229-247.

Azzara, R., A. Basili, L. Beranzoli, C. Chiarabba, R. Di Giovambattista, and G. Selvaggi (1993), The seismic sequenze of Potenza (May 1990), *Annali di Geofisica, 36 (1),* 237-243.

Beneduce, P., and S. I., Giano (1996), Osservazioni preliminari sull'assetto morfostrutturale dell'edificio vulcanico del Monte Vulture (Basilicata), *Il Quaternario, 9 (1),* 325-330.

Billi, A. (2003), Solution slip and separations on strike-slip fault zones: theory and application to the Mattinata Fault, Italy, *Journal of Structural Geology, 25,* 703-715.

Billi, A., and F. Salvini (2000), Sistemi di fratture associati a faglie in rocce carbonatiche: nuovi dati sull'evoluzione tettonica del Promontorio del Gargano, *Boll. Soc. Geol. It., 119,* 237-250.

Borre, K., S. Cacon, G. Cello, B. Kontny, B. Kostak, H. Likke Andersen, G. Moratti, L. Piccardi, J. Stemberk, E. Tondi, and V. Vilimek (2003), The COST project in Italy: analysis and monitoring of seismogenic faults in the Gargano and Norcia areas (central southern Apennines, Italy), *Journal of Geodynamics, 36,* 3-18.

Boschi, E., E. Guidoboni, G. Ferrari, D. Mariotti, G. Valensise, and P. Gasperini, eds. (2000), Catalogue of strong italian earthquakes from 461 B.C. to 1997, *Annals of Geophysics, 43,* 4.

Boschi, E., D. Pantosti, D. Slejko, M. Stucchi, and G. Valensise, eds. (1993), Special issue on the meeting "Irpinia dieci anni dopo", Sorrento 1990, *Annali di Geofisica, 36 (1),* 351 p.

Bosellini, A., C. Neri, and V. Luciani (1993), Guida ai carbonati cretaceo-eocenici di scarpata e bacino del Gargano (Italia meridionale), *Annali dell'Università di Ferrara (Nuova serie), Sezione: Scienze della Terra; vol. 4, Supplemento,* 77 p.

Butler, R. W. H., S. Mazzoli, S. Corrado, M. De Donatis, D. Scrocca, D. Di Bucci, R. Gambini, G. Naso, C. Nicolai, P. Shiner, and V. Zucconi (2004), Applying thick-skinned tectonic models to the Apennine thrust belt of Italy - Limitations and implications. In: McClay, K., ed., Thrust tectonics and hydrocarbon systems, *Am. Ass. Petr. Geol. Memoir, 82,* 647-667.

Calcagnile, G., and G. F. Panza (1981), The main characteristics of the lithosphere-asthenosphere system in Italy and sorrounding regions, *Pure and Applied Geophysics, 119,* 865-879.

Casero, P., F. Roure, L. Endignoux, I. Moretti, C. Muller, L. Sage, and R. Vially (1988), Neogene geodynamic evolution of the southern Apennines, *Mem. Soc. Geol. It., 41,* 109-120.

Casero, P., F. Roure, and R. Vially (1991), Tectonic framework and petroleum potential of the southern Apennines. In: Spencer, A. M., ed., Generation, Accumulation, and Production of Europe's Hydrocarbons, *EAPG Special Publication, 1,* 381-387.

Casnedi, R., and G. Moruzzi (1978), Geologia del campo gassifero di Chieuti (Foggia), *Boll. Soc. Geol. It., 97,* 189-196.

Castello, B., G. Selvaggi, C. Chiarabba, and A. Amato (2005), CSI Catalogo della sismicità italiana 1981-2002, versione 1.0. INGV-CNT, Roma *http://www.ingv.it/CSI/*

Cello, G., I. Guerra, L. Tortorici, E. Turco, R. Scarpa (1982), Geometry of the neotectonic stress field in southern Italy: geological and seismological evidence, *Journal of Structural Geology, 4 (4),* 385-393.

Chiappini, M., A. Meloni, E. Boschi, O. Faggioni, N. Beverini, C. Carmisciano, and I. Marson (2000), Shaded relief magnetic anomaly map of Italy and surrounding marine areas, *Annals of Geophysics, 43 (5),* 983-989.

Chilovi C., A. J. De Feyter, and A. Pompucci (2000), Wrench zone reactivation in the Adriatic Block: the example of the Mattinata Fault System (SE Italy), *Boll. Soc. Geol. It., 119 (1),* 3-8.

Christie-Blick, N., and K. T. Biddle (1985), Deformation and basin formation along strike-slip faults. In: Biddle, K. T., and N. Christie-Blick, eds., Strike-slip deformation, basin formation, and sedimentation, *Society of Economic Paleontologists and Mineralogists, special publication n. 37,* 1-34.

Ciaranfi, N., P. Pieri, and G. Ricchetti, (1988), Note alla carta geologica delle Murge e del Salento (Puglia centromeridionale), *Mem. Soc. Geol. It., 41*, 449-460.

Cinque, A., E. Patacca, P. Scandone, and M. Tozzi (1993), Quaternary kinematic evolution of the southern Apennines. Relationship between surface geological features and deep lithospheric structures, *Annali di Geofisica, 36, (2),* 249-260.

Colantoni, P., M. Tramontana, and R. Tedeschi (1990), Contributo alla conoscenza dell'avampaese apulo: struttura del Golfo di Manfredonia (Adriatico meridionale), *Giornale di Geologia, serie 3a, 52 (1-2),* 19-32.

D'Agostino, N., J. A. Jackson, F. Dramis, and R. Funiciello (2001), Interactions between mantle upwelling, drainage evolution and active normal faulting: an example from the central Apennines (Italy), *Geophysical Journal International 147,* 475-497.

de Alteriis, G. (1995), Different foreland basins in Italy: examples from the central and southern Adriatic Sea, *Tectonophysics, 252,* 349-373.

De' Dominicis, A., and G. Mazzoldi (1987), Interpretazione geologico-strutturale del margine orientale della Piattaforma apula, *Mem. Soc. Geol. It., 38,* 163-176.

Del Gaudio, V., P. Pierri, G. Calcagnile, and N. Venisti (2005), Characteristics of the low energy seismicity of central Apulia (southern Italy) and hazard implications, *Journal of Seismology, 9,* 39-59.

Del Monte, M., D. Di Bucci, and A. Trigari (1996), Assetto morfotettonico della regione compresa tra la Maiella e il Mare Adriatico (Appennino abruzzese), *Mem. Soc. Geol. It., 51,* 419-430.

Demanet, D., L. Margheriti, G. Selvaggi, and D. Jongmans (1998), Upper crustal structure in the Potenza area (Southern Apennines, Italy) using Sp converted waves, *Annali di Geofisica, 41 (1),* 105-119.

DeMets, C., R. G. Gordon, D. F. Argus, and S. Stein (1990), Current plate motions, *Geophys. J. Int., 101,* 425– 478.

Di Bucci, D., and S. Mazzoli (2003), The October-November 2002 Molise seismic sequence (southern Italy): an expression of Adria intraplate deformation, *J. Geol. Soc. London, 160 (4),* 503-506.

Di Luccio, F., E. Fukuyama, and N. A. Pino (2005a), The 2002 Molise earthquake sequence: What can we learn about the tectonics of southern Italy?, *Tectonophysics, 405,* 141-154.

Di Luccio, F., A. Piscini, N. A. Pino, and G. Ventura (2005b), Reactivation of deep faults beneath Southern Apennines: evidence from the 1990–1991 Potenza seismic sequences, *Terra Nova, 00,* 1-5.

Doglioni, C., F. Mongelli, and P. Pieri (1994), The Puglia uplift (SE-Italy): an anomaly in the foreland of the Apenninic subduction due to buckling of a thick continental lithosphere, *Tectonics, 13 (5),* 1309-1321.

Favali, P., R. Funiciello, G. Mattietti, G. Mele, and F. Salvini (1993), An active margin across the Adriatic Sea central Mediterranean Sea), *Tectonophysics, 219,* 109-117.

Ferranti, L., and J. Oldow (2005), Latest Miocene to Quaternary horizontal and vertical displacement rates during simultaneous contraction and extension in the Southern Apennines orogen, Italy, *Terra Nova, 17,* 209-214.

Finetti, I. (1982), Structure, stratigraphy and evolution of the Central Mediterranean, *Boll. Geofis. Teor. Appl., 24,* 247-312.

Funiciello, R., P. Montone, F. Salvini, and M. Tozzi (1988), Caratteri strutturali del Promontorio del Gargano, *Mem. Soc. Geol. It., 41,* 1235-1243.

Galadini, F. (1999), Pleistocene changes in the central Apennine fault kinematics: A key to decipher active tectonics in central Italy, *Tectonics, 18 (5),* 877-894.

Galadini, F., C. Meletti, and A. Rebez, eds. (2000), Le ricerche del GNDT nel campo della pericolosità sismica (1996-1999), *CNR-Gruppo Nazionale per la Difesa dai Terremoti, Roma,* 397 p.

Galli, P., D. Molin, F. Galadini, B. Giaccio (2002), Aspetti sismotettonici del terremoto irpino del 1930. In: Castenetto, S., M. Sebastiano, eds., Il "Terremoto del Vulture", *Presidenza del Consiglio, Dipartimento della Protezione Civile, Servizio Sismico Nazionale*, Roma, 217-262.

Gasparini, C., G. Iannaccone, and R. Scarpa (1985), Fault-plane solutions and seismicity of the Italian peninsula, *Tectonophysics, 117,* 59-78.

Giuliani, R., M. Anzidei, L. Bonci, S. Calcaterra, G. Casula, N. D'Agostino, A. Esposito, F. Loddo, M. Mattone, G. Pietrantonio, F. Riguzzi, and G. Selvaggi (2003), Terremoto del Molise del 31 Ottobre 1 Novembre 2002: campo di deformazione cosismica da misure GPS, *22° Convegno Nazionale GNGTS, Riassunti estesi delle comunicazioni,* 145-147.

Gruppo di Lavoro CPTI (1999), Catalogo Parametrico dei Terremoti Italiani, *ING – GNDT – SGA – SSN*, Bologna, 92 p.

Harding, T. P. (1985), Seismic characteristics and identification of negative flower structures, positive flower structures, and positive structural inversion, *Am. Ass. Petr. Geol. Bulletin, 69 (4),* 582-600.

Hollenstein, Ch., H.-G. Kahle, A. Geiger, S. Jenny, S. Goes, and D. Giardini (2003), New GPS constraints on the Africa-Eurasia plate boundary zone in southern Italy, *Geophys. Res. Lett., 30 (18),* 1935, 10.1029/2003GL017554.

Hubbert, M. K. (1937), Theory of scale models as applied to the study of geological structures, *Geological Society of America Bulletin, 48,* 1459-1520.

Kim, Y.-S., D. C. P., Peacock, and D. J., Sanderson (2004), Fault damage zones, *Journal of Structural Geology, 26,* 503-517.

Lavecchia, G. (1988), The Tyrrhenian-Apennines system: structural setting and seismotectogenesis, *Tectonophysics, 147,* 263-296.

Lopes Cardozo, G., G. Bada, A. Lankreijer, and D. Nieuwland (2002), Analogue modeling of a prograding strike-slip fault: case study of the Balatonfo fault, western Hungary, *EGU Stephan Mueller Special Publication Series, 3,* 217-226.

Mandl, G. (1988), *Mechanics of tectonic faulting: Models and basic concepts,* 407 pp., Elsevier, Netherlands.

Mandl, G., (2000), *Faulting in Brittle Rocks,* 434 pp., Springer, Berlin.

Mariotti, G., and C. Doglioni (2000), The dip of the foreland monocline in the Alps and Apennines, *Earth and Planetary Science Letters, 181,* 191-202.

McClusky, S., R. Reilinger, S. Mahmoud, D. Ben Sari, and A. Tealeb (2003), GPS constraints on Africa (Nubia) and Arabia plate motions, *Geophysical Journal International, 155 (1),* 126-138.

Menardi Noguera, A., and G. Rea (2000), Deep structure of the Campanian-Lucanian Arc (southern Apennines), *Tectonophysics, 324,* 239-265.

Montone, P., A. Amato, and S. Pondrelli (1999), Active Stress Map of Italy, *Journ. Geophys. Res. 104 (B11),* 25,595-25,610.

Montone, P., M. T. Mariucci, S. Pondrelli, and A. Amato (2004), An improved stress map for Italy and surrounding regions (central Mediterranean), *Journal of Geophysical Research, 109 (B10410),* 1-22, doi: 10.1029/1003JB002703.

Morelli, D. (2002), Evoluzione tettonico-stratigrafica del Margine Adriatico compreso tra il Promontorio garganico e Brindisi, *Mem. Soc. Geol. It., 57,* 343-353.

Mostardini, F., and S. Merlini (1986), Appennino centro-meridionale. Sezioni Geologiche e Proposta di Modello Strutturale, *Mem. Soc. Geol. It., 35,* 177-202.

Naylor, M. A., G. Mandl, and C. H. K. Sijpesteijn (1986), Fault geometries in basement-induced wrench faulting under different initial stress states, *Journal of Structural Geology, 8,* 737-752.

Nieuwland, D. A., and M. Nijman (2001), The atlas of structural geometry: a digital collection of 25 years of analogue modelling, *Geologie en Mijnbouw / Netherlands Journal of Geosciences, 80,* 59-60.

Patacca, E., and P. Scandone (1989), Post-Tortonian mountain building in the Apennines. The role of the passive sinking of a relic lithospheric slab. In: Boriani, A., M. Bonafede, G. B. Piccardo, and G. B. Vai, eds., The Lithosphere in Italy, *Atti dei Convegni Lincei, 80,* 157-176.

Patacca, E., and P. Scandone (2004a), The 1627 Gargano earthquake (Southern Italy): Identification and characterization of the causative fault, *Journal of Seismology, 8 (2),* 259-273.

Patacca, E., and P. Scandone (2004b), The Plio-Pleistocene thrust belt – foredeep system in the Southern Apennines and Sicily (Italy). In: Crescenti, U., S. D'Offizi, S. Merlini, and L. Lacchi, eds., Geology of Italy, Società Geologica Italiana, Roma, 232 pp.

Patacca, E., P. Scandone, and M. Tozzi (2000), Il profilo CROP04, *Protecta, 10-12,* 49-52.

Piccardi, L. (1998), Cinematica attuale, comportamentosismico e sismologia storica della faglia di Monte Sant'angelo (Gargano, Italia): la possibile rottura superficiale del "leggendario" terremoto del 493 d.C., *Geogr. Fis. Dinam. Quat., 21,* 155-166.

Piccardi, L. (2005), Paleoseismic evidence of legendary earthquakes: The apparition of Archangel Michael at Monte Sant'Angelo (Italy), *Tectonophysics, 408,* 113–128

Pondrelli, S., F. Di Luccio, E. Fukuyama, S. Mazza, M. Olivieri, and N. A. Pino (2003), Fast determination of moment tensors for the recent Molise (southern Italy) seismic sequence, *ORFEUS Newsletter, 5 (1).*

Ramberg, H. (1981), *Gravity, deformation Earth's crust*, 452 pp., Academic Press, London.

Ricchetti, G., N. Ciaranfi, E. Luperto Sinni, F. Mongelli, P. Pieri (1988), Geodinamica ed evoluzione sedimentaria e tettonica dell'avampaese apulo, *Mem. Soc. Geol. It., 41*, 57-82.

Richard, P. D., and P. Cobbold (1990), Experimental insights into partitioning of fault motions in continental convergent wrench zones, *Annales Tectonicae, Special Issue, 4 (2),* 35-44.

Richard, P. D., M. A. Naylor, and A. Koopman (1995), Experimental models of strike slip tectonics, *Petroleum Geoscience, 1,* 71-80.

Richard, P., and R. W. Krantz (1991), Experiments on fault reactivation in strike-slip mode, *Tectonophysics, 188,* 117-131.

Sassi, W., B. Colletta, P. Balé, and T. Paquereau (1993), Modelling of structural complexity in sedimentary basins: the role of pre-existing faults in thrust tectonics, *Tectonophysics, 226,* 97-112.

Schellart, W. P. (2000), Shear test results for cohesion and friction coefficients for different granular materials: scaling implications for their usage in analogue modelling, *Tectonophysics, 324,* 1–16.

Schöpfer, M. P. J., and H. P. Steyrer (2001), Experimental modeling of strike-slip faults and the self-similar behavior. In: Koyi, H. A., and N. S. Mancktelow, eds., Tectonic Modeling: A Volume in Honor of Hans Ramberg, *Geological Society of America Memoir, 193,* 21-27.

S.G.N., Servizio Geologico Nazionale, (1965), Carta geologica d'Italia, scale 1:100.000, Sheet 157 "Monte S. Angelo", II edition.

S.G.N., Servizio Geologico Nazionale, (1970), Carta geologica d'Italia, scale 1:100,000, Sheet 156 "S. Marco in Lamis", II edition.

Sylvester, A. G. (1988), Strike-slip faults, *Geol. Soc. Am. Bull., 100,* 1666-1703.

Tchalenko, J. S. (1970), Similarities between shear zones of different magnitudes, *Geol. Soc. Am. Bull., 81,* 1625-1640.

Tiberti M. M., L. Orlando, D. Di Bucci, M. Bernabini, and M. Parotto (2005), Regional gravity anomaly map and crustal model of the.Central-Southern Apennines (Italy), *Journal of Geodynamics, 40,* 73-91.

Turrini, C., A. Ravaglia, and C. R. Perotti (2001), Compressional structures in a multilayered mechanical stratigraphy: insights from sandbox modelling with three-dimensional variations in basal geometry and friction. In: Koyi, H. A., and N. S. Mancktelow, eds., Tectonic

Modeling: A Volume in Honor of Hans Ramberg, *Geological Society of America Memoir, 193,* 153-178.

Ueta, K., K. Tani, and T. Kato (2000), Computerized X-ray tomography analysis of three-dimensional fault geometries in basement-induced wrench faulting, *Engineering Geology, 56,* 197-210.

Valensise, G., and D. Pantosti, eds. (2001), Database of Potential Sources for Earthquakes Larger than M 5.5 in Italy, *Annals of Geophysics, 44 (1),* with CD-ROM.

Valensise, G., D. Pantosti, and R. Basili (2004), Seismology and Tectonic Setting of the Molise Earthquake Sequence of October 31-November 1, 2002, *Earthq. Spectra, 20 (1),* 23-37.

Viola, G., F. Odonne, and N. S. Mancktelow (2004), Analogue modelling of reverse fault reactivation in strike-slip and transpressive regimes: application to the Giudicarie fault system, Italian Eastern Alps, *Journal of Structural Geology, 36,* 401-418.

Ward, S. N. (1994), Constraints on the seismotectonics of the central Mediterranean from Very Long Baseline Interferometry, *Geophys. J. Int., 117,* 441-452.

Wilcox, R. E., T. P. Harding, and D. R. Seely (1973), Basic wrench tectonics, *The American Association of Petroleum Geologists Bulletin, 57 (1),* 74-96.

Winter, T., and P. Tapponnier (1991), Extension majeure post-Jurassique et ante-Miocene dans le centre de l'Italie: données microtectoniques, *Bull. Soc. Géol., France, 162 (6),* 1095-1108.

Zarraoa, N., A. Rius, E. Sardón, and J. W. Ryan (1994), Relative motions in Europe studied with a geodetic VLBI network, *Geophys. J. Int., 117,* 763-768.

Figure and table captions

Figure 1. Geological sketch map of peninsular Italy from the Po Plain to the north of the Calabrian arc [after *Butler et al.*, 2004, modified], showing location of Figures 2 and 3 and of the modeled area. The Mattinata-Gondola shear zone (MGsz) is also shown.

Figure 2. Seismicity and σ_{hmin} of the Central and Southern Apennines [*Gruppo di lavoro CPTI*, 1999; *Montone et al*., 1999; *Valensise and Pantosti eds.*, 2001, and references therein]. The size of the square symbols is proportional to an equivalent magnitude derived from intensity data. Focal mechanisms of selected events (with year and magnitude) after *Cello et al.* [1982], *Gasparini et al.* [1985], *Boschi et al. eds.* [1993], *Demanet et al.* [1998], *Pondrelli et al.* [2003], *Del Gaudio et al.* [2005], *Di Luccio et al.* [2005a]. See Figure 1 for the location. In particular, the focal mechanisms marked "2002" refer to the 31 October-1 November 2002 Molise earthquakes, and that marked "1990" refers to the 5 May 1990 Potenza earthquake.

Figure 3. Schematic structural cross-section across the study area [after *Menardi Noguera and Rea*, 2000, simplified and redrawn]. See Figure 1 for location. Instrumental seismicity of the Southern Apennines is also shown (after *Valensise et al.* [2004], redrawn). The 2002 earthquakes fall in the crustal volume outlined by a dashed line in the cross-section. Notice that the sequence took place at a depth in the range 10-24 km. The thickness of the seismogenic layer is of ca. 20-25 km.

Figure 4. Sketch of the experimental set-up. Two fixed sidewalls confine the sand parallel to the strike-slip motion, whereas the model is open on the other two sides. The three regional-scale domains discussed in the text are indicated (**A**, **B**, **C**).

Figure 5. Interpreted plan-views of the deformation kinematics of reference model SS02 (left; a-h) and model SS03 (right; i-s). Reference vertical lines are spaced ca. 5.5 cm. The horizontal hatched line is the baseplate fault, BF. In model SS03 (i), the dotted line represents the pre-existing fault, P, buried under the front of the Apennine chain. Labels **A**, **B** and **C** mark the three regional-scale domains (see Figure 4). Final displacement was D = 8.0 cm. The newly formed faults are indicated with an arrow showing the sense of propagation through the sand surface. They strictly refer to the specific step shown (in plan-view, deformation kinematics was analyzed at every 0.5 cm step of basal displacement).

Figure 6. Interpreted map-view and cross sections of model SS06. Final displacement was D = 0.5 cm. In plan view, the E-W dotted line is the surface projection of the baseplate fault, whereas the hatched lines represent faults or part of them that do not reach the surface. P marks the pre-existing fault, both exposed and buried under the front of the Apennine chain. Labels **A**, **B** and **C** indicate the three regional-scale domains (see Figure 4). The two layers of glass microbeads are also indicated.

Figure 7. Interpreted map-view and cross sections of model SS05. Final displacement was D = 3.0 cm. In plan view, the E-W dotted line is the surface projection of the baseplate fault, whereas the hatched lines represent faults or part of them that do not reach the surface. P marks the pre-existing fault, both exposed and buried under the front of the Apennine chain. Labels **A**, **B** and **C** indicate the three regional-scale domains (see Figure 4). The two layers of glass microbeads are also indicated.

Figure 8. Interpreted map-view and cross sections of model SS04. Final displacement was D = 5.5 cm. In plan view, the E-W dotted line is the surface projection of the baseplate fault, whereas the hatched lines represent faults or part of them that do not reach the surface. P marks the pre-existing fault, both exposed and buried under the front of the Apennine chain. Labels **A**, **B** and **C** indicate the three regional-scale domains (see Figure 4). The two layers of glass microbeads are also indicated. **a** and **b** mark truly blind faults.

Figure 9. Interpreted map-view and cross sections of model SS03. Final displacement was D = 8.0 cm. In plan view, the E-W dotted line is the surface projection of the baseplate fault, whereas the hatched lines represent faults or part of them that do not reach the surface. P marks the pre-existing fault, both exposed and buried under the front of the Apennine chain. Labels **A**, **B** and **C** indicate the three regional-scale domains (see Figure 4). The two layers of glass microbeads are also indicated.

Figure 10. Sketch of the deformation mechanism of a fault (s) developed in domain **B** (for instance, fault #5 in model SS04, Figure 8). Fault attitude, depth and kinematics change along strike. The resulting mechanism is that of a scissor fault, that also produces vertical relative motion of the ground surface.

Figure 11. Modeling results compared with corresponding spots on the MGsz (all taken from literature, modified and redrawn as needed). Please, note that the models' sections are shown mirror-like (i.e. as seen from the east) with respect to the previous figures, in order to compare them with the existing geological sections. Three of these geological sections are at regional scale, and the oblique orientation with respect to the sections of the models does not invalidate the observed analogies. Dark grey refers to the chain, the frontal wedge and the foredeep deposits. Light grey refers to the foreland.

- s66 mod SS06. Foreland domain **A**; pre-existing cut comparable with the Mattinata fault.

  a1, ***a2***. Geological sections across the Mattinata fault [*S.G.N.*, 1975; 1970]. Note the continuous and well defined setting of the fault for all its length.
- s54 mod SS06. Wedge domain **B**; faults formed in the northern block (trace length 15 cm ca.) are similar to the Apricena fault.

  b. Geological section across the Apricena fault and Chieuti high [*Patacca and Scandone*, 2004a].
- s48 mod SS06. Wedge domain **B**; deep fault comparable with the 2002 Molise seismogenic source.

  c. Regional section crossing the epicentral area of the 2002 Molise earthquakes [*Mostardini and Merlini*, 1986].
- s44 mod SS06. Wedge domain **B**; structural setting comparable to that of the 1990 Potenza sequence.

  d. Regional section across the westernmost part of the study area [*Butler et al.*, 2004]. The geological setting is comparable to that of the region hit by the 1990 Potenza sequence (that is located about 150 km to the southeast of the MGsz). The projection of the 2002 Molise sequence focal volume is highlighted by the dashed ellipse.

Table 1. Stratigraphy of the Apulia Platform and underlying basement.

Table 2. Scaling of the models vs. geological parameters.

Table 3. List of the experiments described in this study and of their geometrical parameters.

Table 1. Stratigraphy of the Apulia Platform and underlying basement.

Age	Lithology	Thickness (when present, names refer to deep wells)	Reference
Tertiary	Open shelf carbonate deposits.	500 m	*Ciaranfi et al.* [1988]
Upper Cretaceous	Mudstone, wackstone, fossiliferous patch reef facies.	700 m	*Ciaranfi et al.* [1988]
Jurassic and Lower Cretaceous	Fossiliferous packstone/wackstone, dolomite, dolomite breccia, mudstone.	Puglia 1 = 3500 m	*Butler et al.* [2004]
	Limestone and dolomite.	Ugento 1 = 4532 m Canosa 9 = 4000 m Sannicandro 1, Foresta U. 1, Peschici 1, Gargano 1 = 3000-3500 m	*Bosellini et al.* [1993]
Upper Trias (Raethian)	Fractured dolomite.	Puglia 1 = 1500 m	*Butler et al.* [2004]
	Dolomite.	Gargano 1 = 850 m Foresta U. 1 = 1200 m	*Bosellini et al.* [1993]
Upper Trias (Norian)	White crystalline anhydrite interbedded with dark grey dolomite, oolithic in places.	Puglia 1 = 1070 m	*Butler et al.* [2004]
	Dolomite-evaporite complex.	Gargano 1 = 2000 m Foresta U. 1 = 2621 m	*Bosellini et al.* [1993]
	"Anidriti di Burano" Fm. s.s.	Gargano 1 = 400 m Foresta U. 1 = 2621 m G.E.M. 1 = 200 m	
Lower Trias and Carnian	Polygenic breccia in red argillaceous matrix with thin interbeds of red silty shale.	Puglia 1 = 185 m	*Butler et al.* [2004]
	Dolomite, anhydrite, red shale, conglomerate ("Verrucano" Fm.).	Gargano 1 = 492 m	*Bosellini et al.* [1993]
Upper Permian	Gray sandstone with siliceous/carbonatic cement, with thin mudstone stringers and rare breccia.	Puglia 1 = 1000 m	*Butler et al.* [2004]
Lower Permian	Metapelite (low grade metamorphism), white dolomite, conglomerate, limestone, igneous bodies.	Gargano 1 = 311 m	*Bosellini et al.* [1993]

Table 2. Scaling of the models vs. geological parameters.

Analogue models SS03 to SS06	Geological reference
Model length = more than 100 cm	MGsz minimum length = 180 km + 10-15 km
Model width = 50 cm (to avoid lateral effects)	MGsz width = ca. 15 km
Minimum thickness (foreland-side)= 10 cm	Seismogenic layer in the foreland = 20 km
Maximum thickness (orogenic wedge-side) = 11 cm	2000 m of topographic relief are added in the orogenic wedge area = 22 km
Dip angle of the wedge = ca. 20°	After published regional geological cross-sections [C*asero et al.*, 1988; 1991; *Patacca et al.*, 2000; *Menardi Noguera and Rea*, 2000; *Butler et al.*, 2004]
0.5 cm-thick layer of glass microbeads at 3.5 km depth in the foreland-side of the model	ca. 1000 m thick anhydrite-dolomite deposits at the bottom of the Apulia Platform succession (total thickness = 6000 m)
0.3 cm ca. thick layer of glass microbeads between the wedge and the underlying foreland	It simulates the physical discontinuity between the orogenic wedge and the underlying foreland
Right-lateral baseplate fault, in the middle of the model and perpendicular to the wedge front	Crustal wrench zone with right-lateral sense of motion
Vertical discontinuity = a cut in the foreland-side and below the wedge (that is not cut), made by means of 0.5 mm thick nylon thread located in correspondence with the baseplate fault	MGsz activity dated back to Mesozoic times. The orogenic wedge reached the present-day location in Middle Pleistocene
Minimum right-lateral displacement = 0.5 cm	Horizontal slip rate 1.0 mm/a after *Piccardi* [1998]; cumulative since Middle Pleistocene = less than 1 km
Maximum right-lateral displacement = 8.0 cm	15 km, after *De' Dominicis and Mazzoldi* [1987] and *Chilovi et al.* [2000]

Table 3. List of the experiments described in this study and of their geometrical parameters.

Experiment	Pre-existing cut	Layer of glass microbeads in the foreland	Presence of the wedge	Thickness	Displacement
SS02	No	No	No	10 cm	8.0 cm
SS03	Yes	Yes	Yes	10-11 cm	8.0 cm
SS04	Yes	Yes	Yes	10-11 cm	5.5 cm
SS05	Yes	Yes	Yes	10-11 cm	3.0 cm
SS06	Yes	Yes	Yes	10-11 cm	0.5 cm

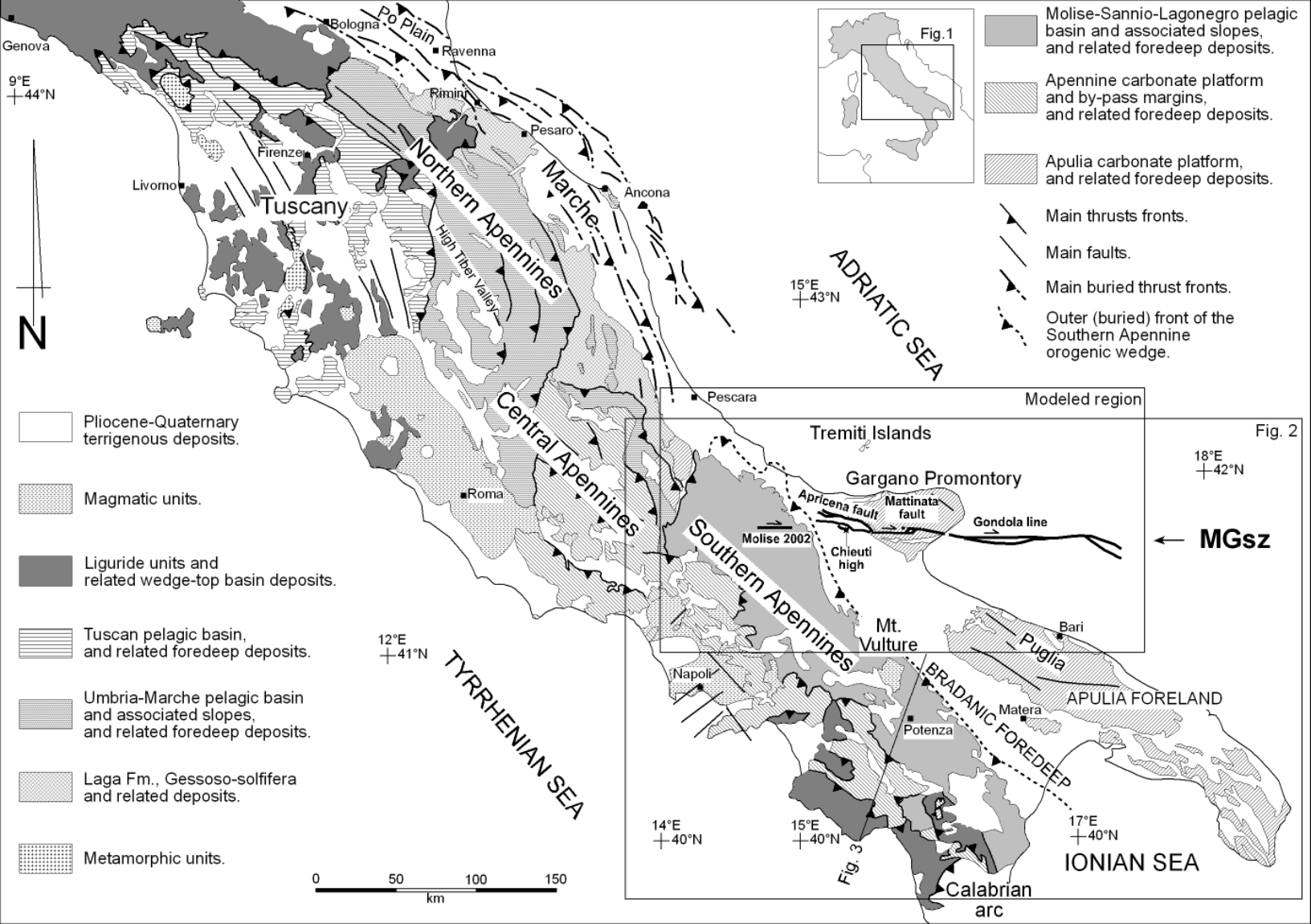
Genova
Bologna
Po Plain
Ravenna
Rimini
Pesaro
Ancona
Firenze
Livorno
Tuscany
Northern Apennines
High Tiber Valley
Marche
ADRIATIC SEA
Central Apennines
Roma
Pescara
Modeled region
Fig. 2
Tremiti Islands
Gargano Promontory
Apricena fault
Mattinata fault
Gondola line
Molise 2002
Chieuti high
MGsz
Southern Apennines
Mt. Vulture
Bari
Puglia
Napoli
BRADANIC FOREDEEP
APULIA FORELAND
Matera
Potenza
TYRRHENIAN SEA
IONIAN SEA
Calabrian arc
Fig. 3
Fig.1
9°E 44°N
12°E 41°N
14°E 40°N
15°E 40°N
15°E 43°N
17°E 40°N
18°E 42°N
N
0 50 100 150 km
Molise-Sannio-Lagonegro pelagic basin and associated slopes, and related foredeep deposits.
Apennine carbonate platform and by-pass margins, and related foredeep deposits.
Apulia carbonate platform, and related foredeep deposits.
Main thrusts fronts.
Main faults.
Main buried thrust fronts.
Outer (buried) front of the Southern Apennine orogenic wedge.
Pliocene-Quaternary terrigenous deposits.
Magmatic units.
Liguride units and related wedge-top basin deposits.
Tuscan pelagic basin, and related foredeep deposits.
Umbria-Marche pelagic basin and associated slopes, and related foredeep deposits.
Laga Fm., Gessoso-solfifera and related deposits.
Metamorphic units.

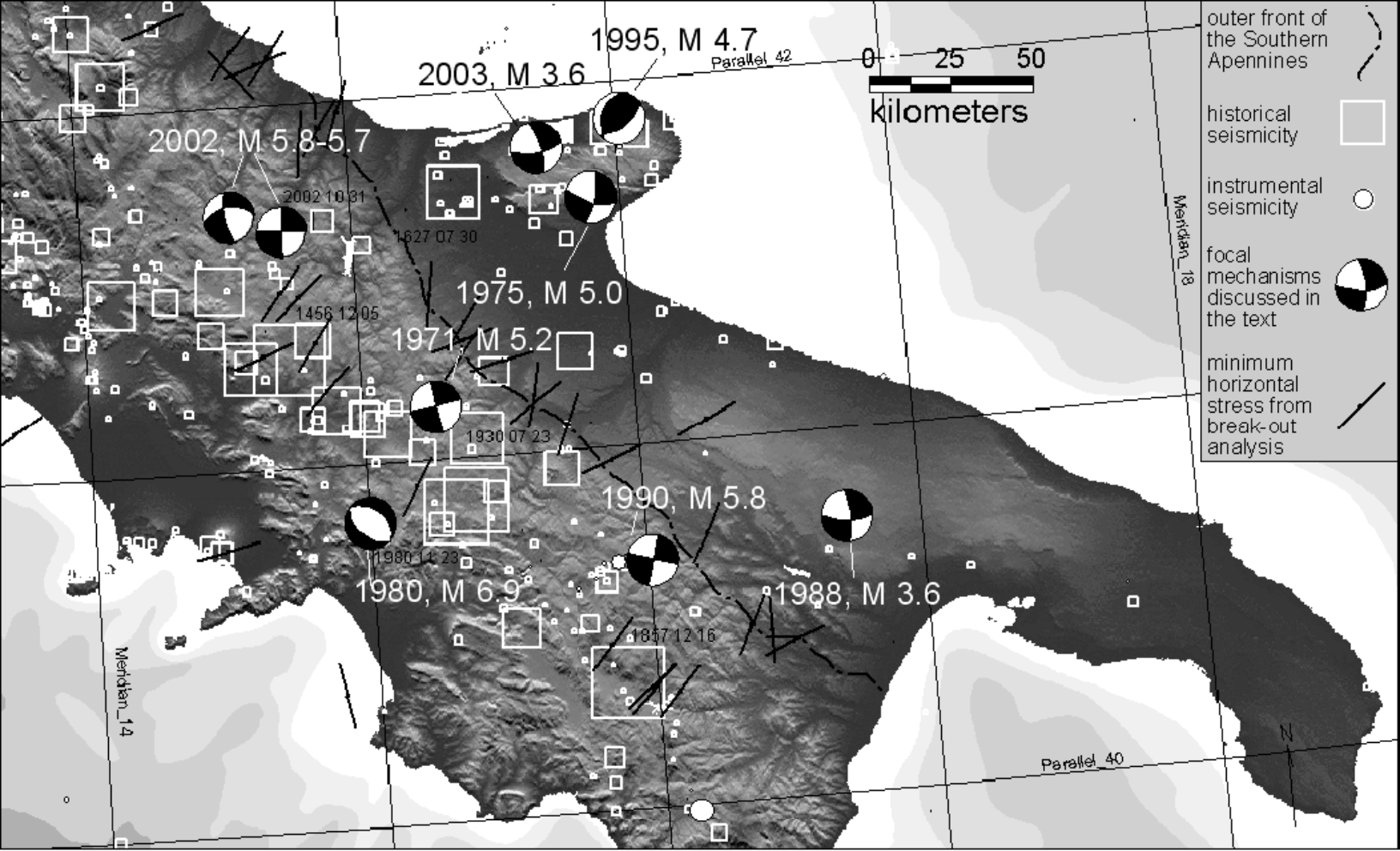
1995, M 4.7
2003, M 3.6
2002, M 5.8-5.7
2002 10 31
1627 07 30
1456 12 05
1975, M 5.0
1971, M 5.2
1930 07 23
1990, M 5.8
1980, M 6.9
1980 11 23
1988, M 3.6
1857 12 16
Parallel_42
Parallel_40
Meridian_14
Meridian_18
0 25 50
kilometers
N
outer front of the Southern Apennines
historical seismicity
instrumental seismicity
focal mechanisms discussed in the text
minimum horizontal stress from break-out analysis

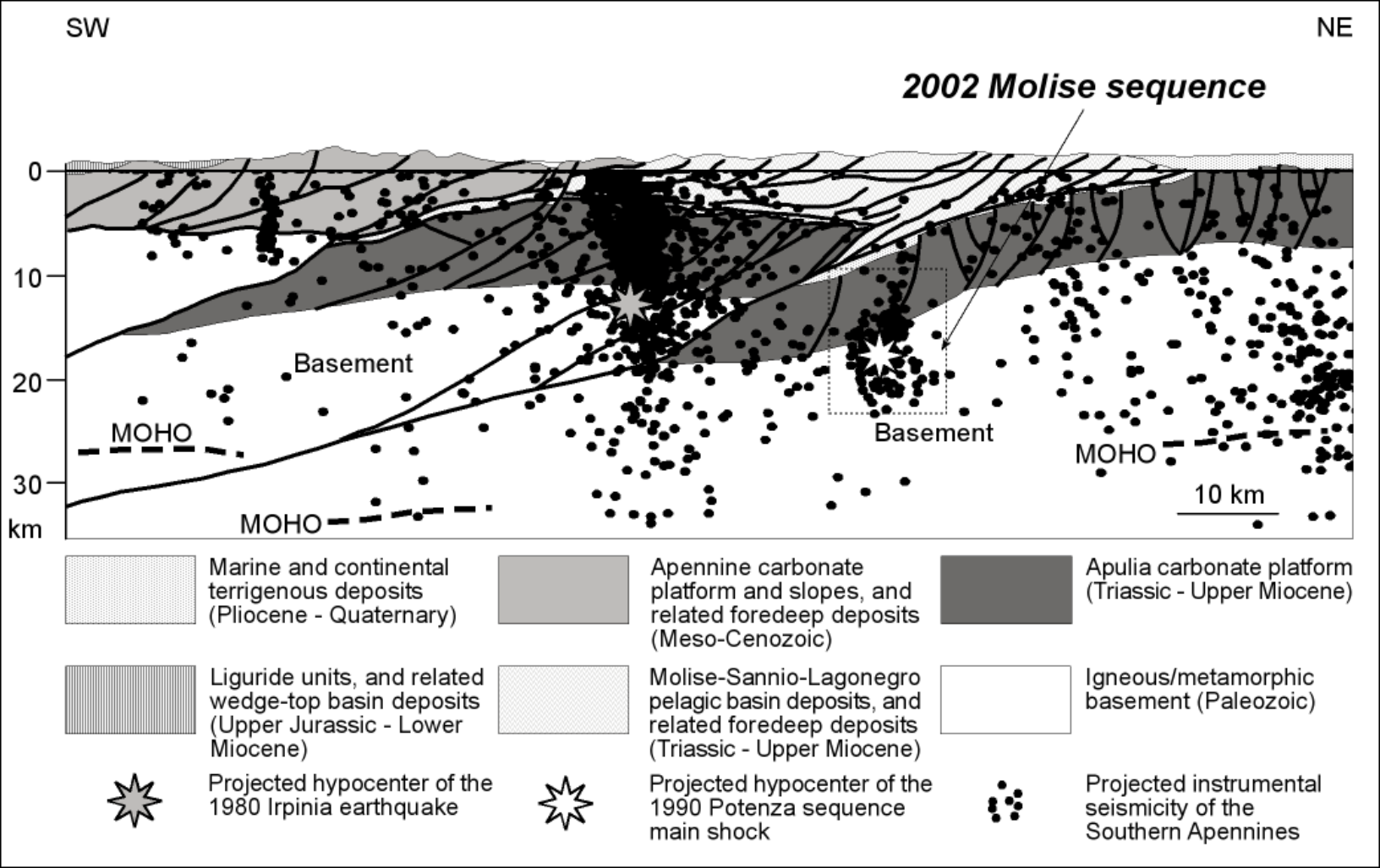
SW
NE
2002 Molise sequence
0
10
20
30
km
Basement
MOHO
MOHO
Basement
MOHO
10 km
Marine and continental terrigenous deposits (Pliocene - Quaternary)
Apennine carbonate platform and slopes, and related foredeep deposits (Meso-Cenozoic)
Apulia carbonate platform (Triassic - Upper Miocene)
Liguride units, and related wedge-top basin deposits (Upper Jurassic - Lower Miocene)
Molise-Sannio-Lagonegro pelagic basin deposits, and related foredeep deposits (Triassic - Upper Miocene)
Igneous/metamorphic basement (Paleozoic)
Projected hypocenter of the 1980 Irpinia earthquake
Projected hypocenter of the 1990 Potenza sequence main shock
Projected instrumental seismicity of the Southern Apennines

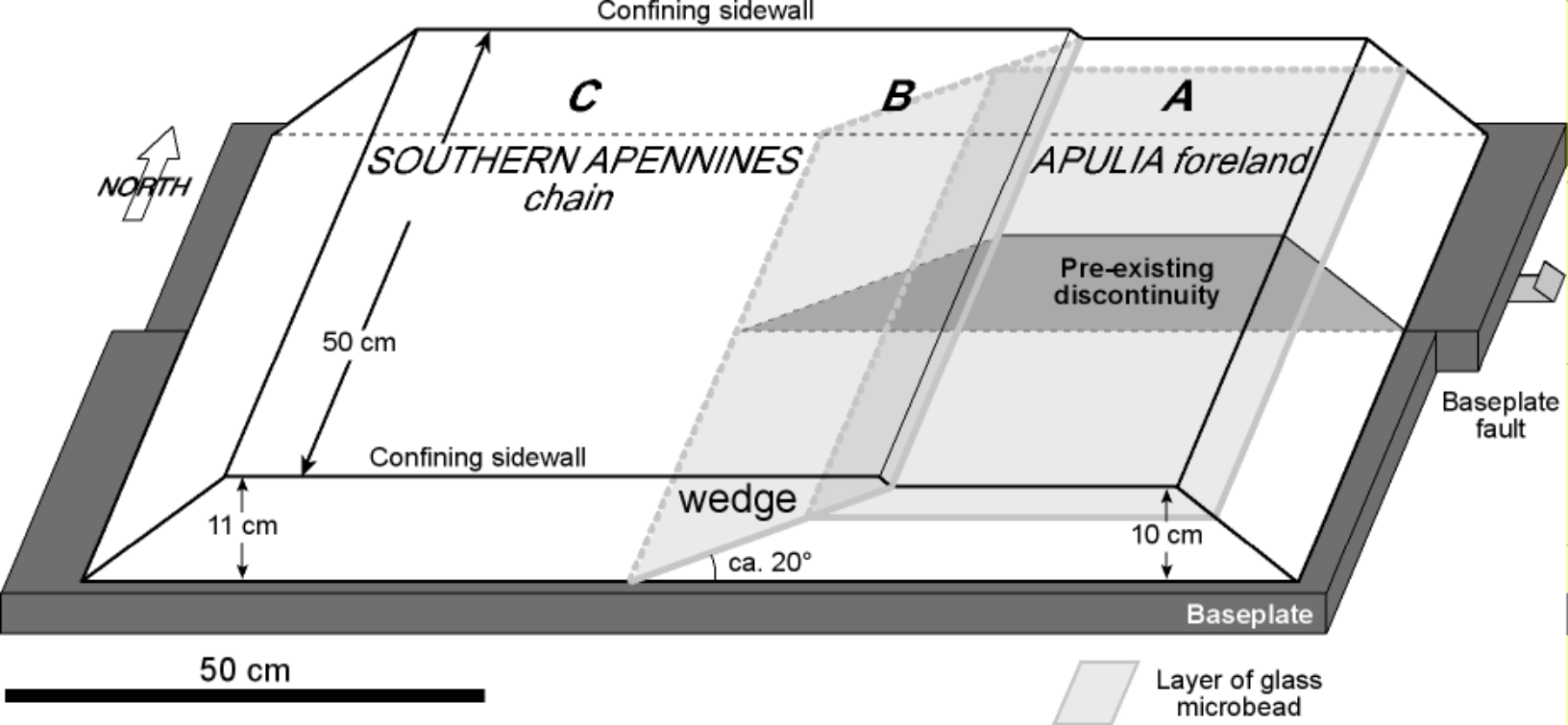
Confining sidewall
C
B
A
NORTH
SOUTHERN APENNINES
chain
APULIA foreland
Pre-existing
discontinuity
50 cm
Baseplate
fault
Confining sidewall
wedge
11 cm
10 cm
ca. 20°
Baseplate
50 cm
Layer of glass
microbead

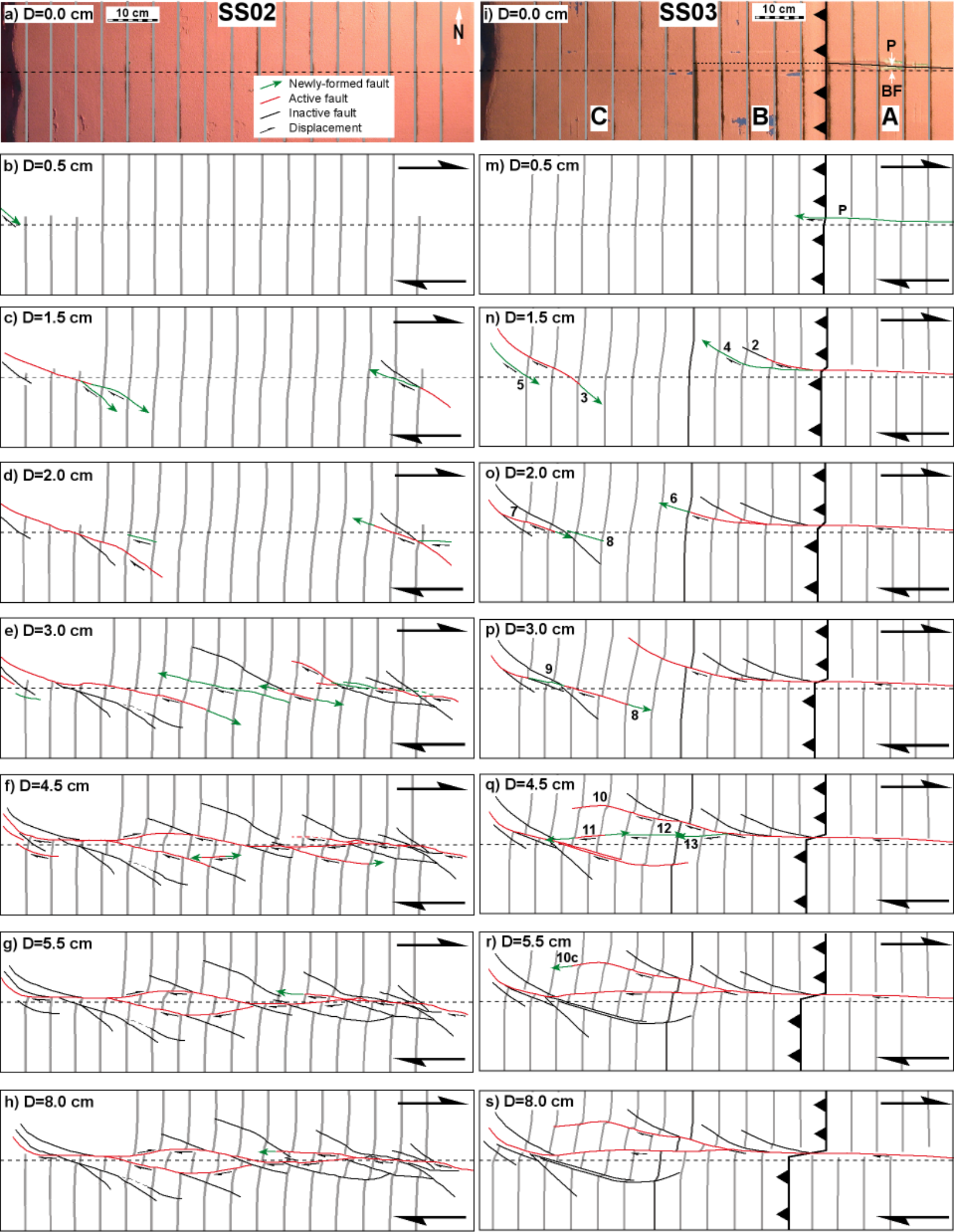
a) D=0.0 cm
10 cm
SS02
N
Newly-formed fault
Active fault
Inactive fault
Displacement
i) D=0.0 cm
SS03
10 cm
P
BF
C
B
A
b) D=0.5 cm
m) D=0.5 cm
P
c) D=1.5 cm
n) D=1.5 cm
4
2
5
3
d) D=2.0 cm
o) D=2.0 cm
6
7
8
e) D=3.0 cm
p) D=3.0 cm
9
8
f) D=4.5 cm
q) D=4.5 cm
10
11
12
13
g) D=5.5 cm
r) D=5.5 cm
10c
h) D=8.0 cm
s) D=8.0 cm

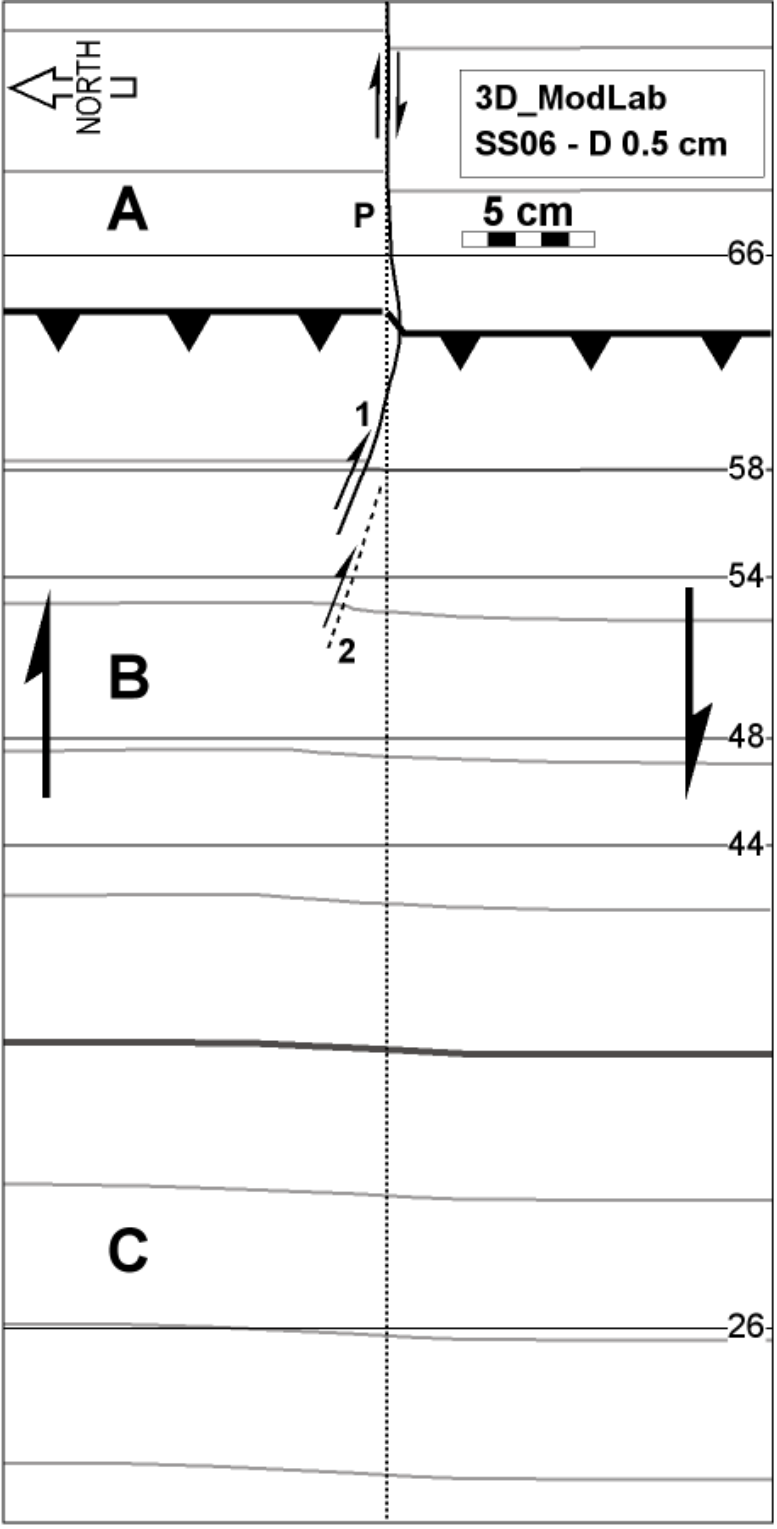
NORTH
3D_ModLab
SS06 - D 0.5 cm
A
P
5 cm
66
1
58
54
2
B
48
44
C
26

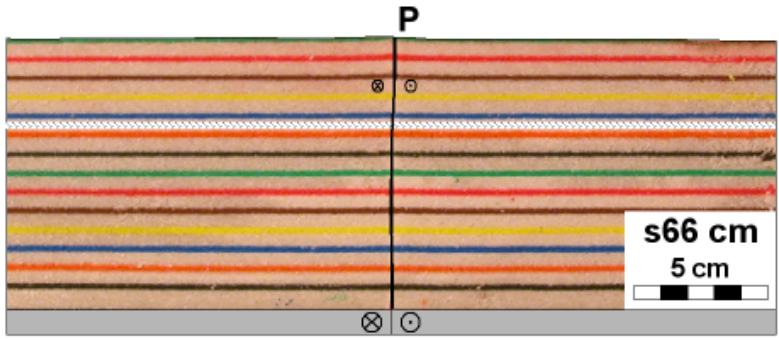
P
s66 cm
5 cm

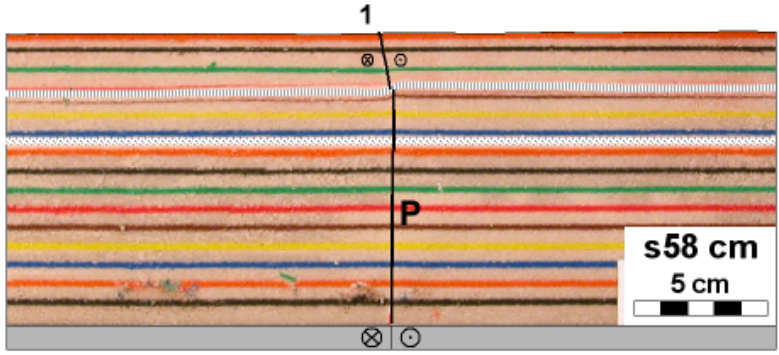
1
P
s58 cm
5 cm

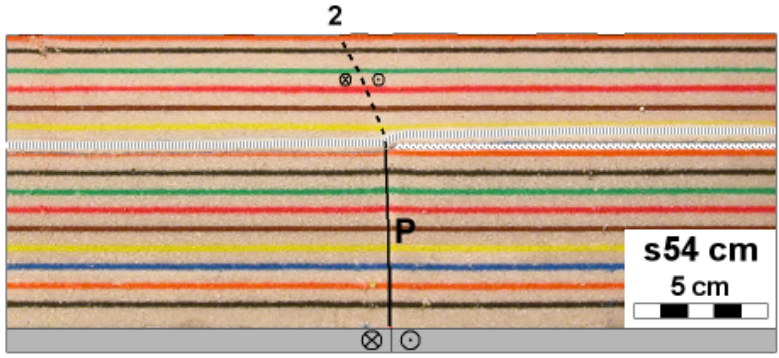
2
P
s54 cm
5 cm

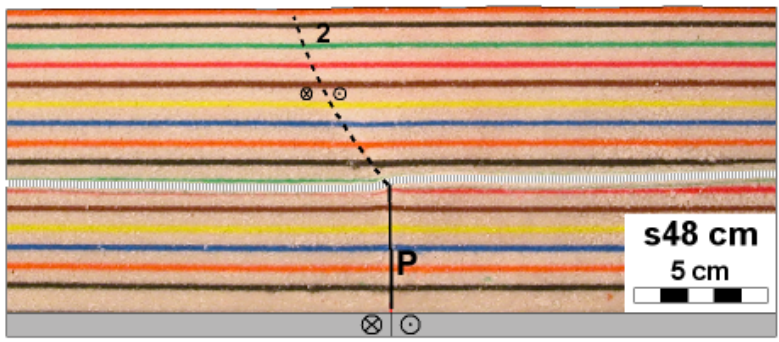
2
P
s48 cm
5 cm


s26 cm
5 cm

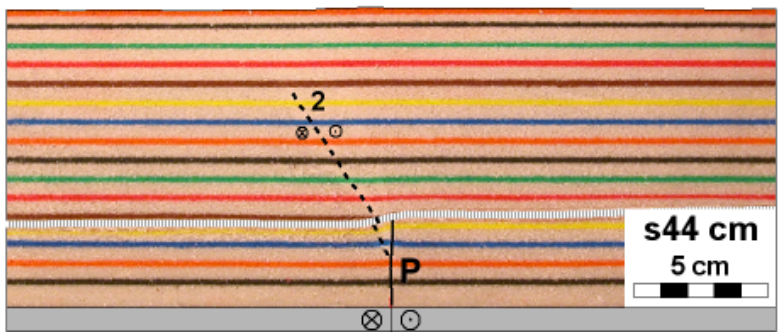
2
P
s44 cm
5 cm

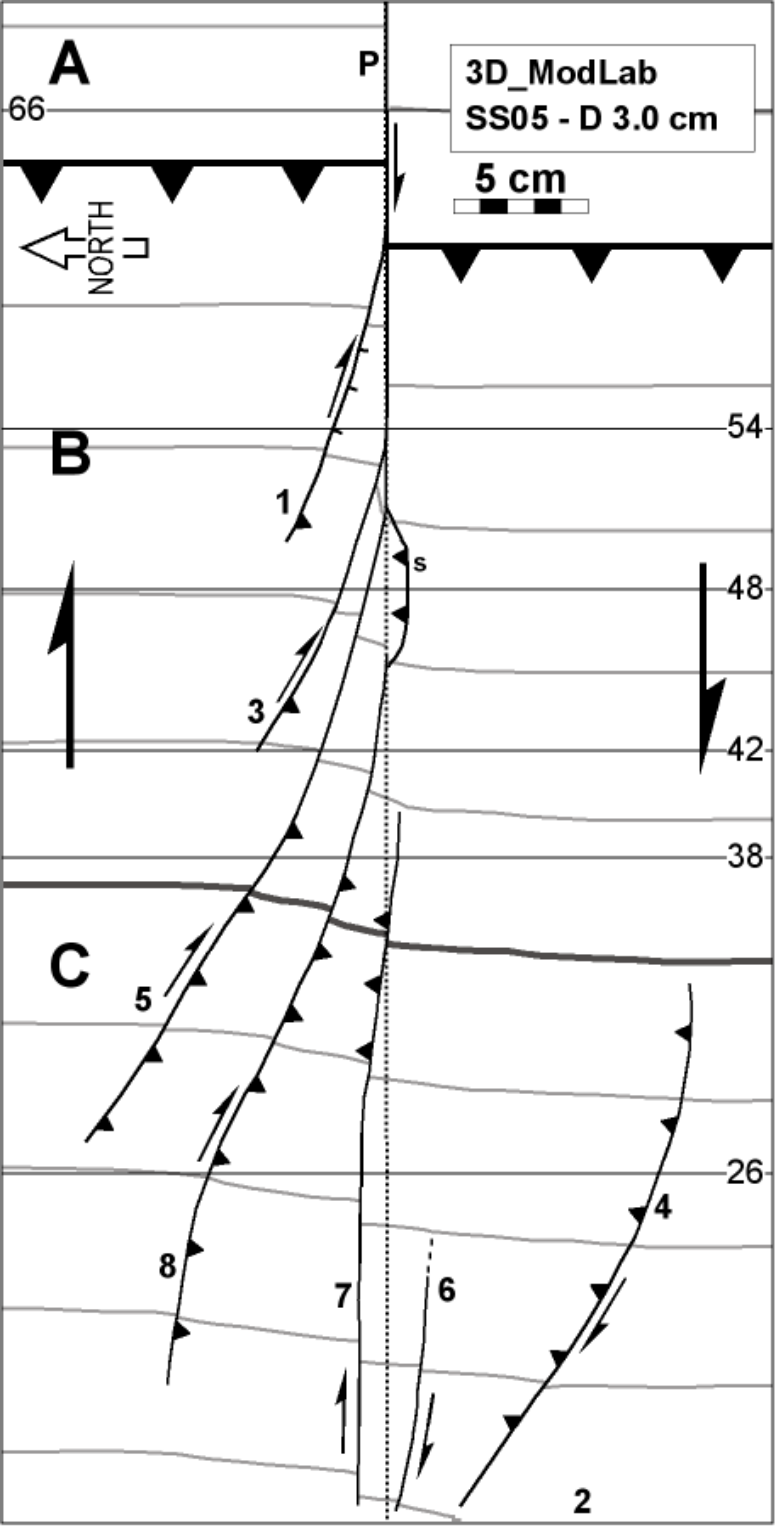
A
P
66
3D_ModLab
SS05 - D 3.0 cm
5 cm
NORTH
B
54
1
s
48
3
42
38
C
5
26
8
7
6
4
2

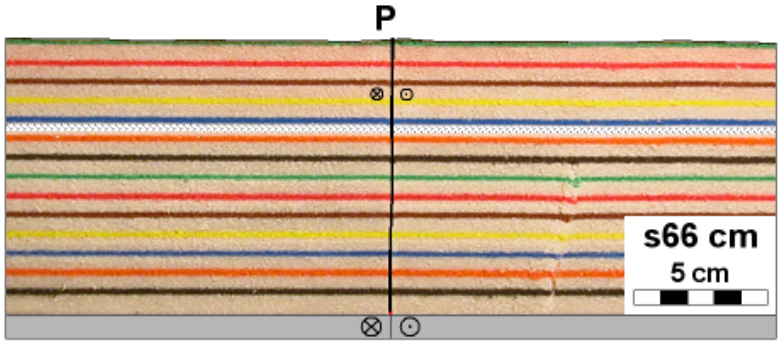
P
s66 cm
5 cm

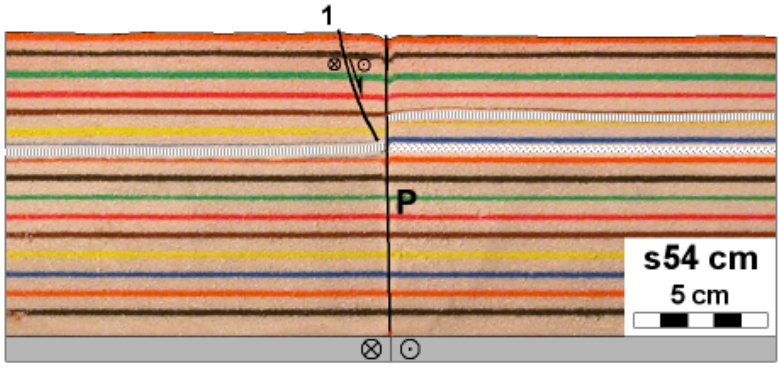
1
P
s54 cm
5 cm

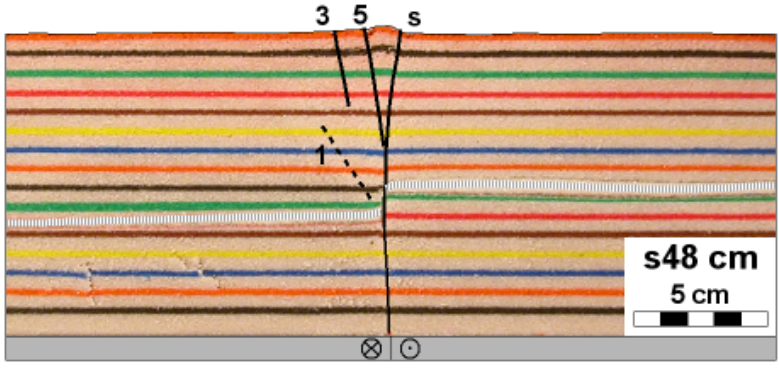
3
5
s
1
s48 cm
5 cm

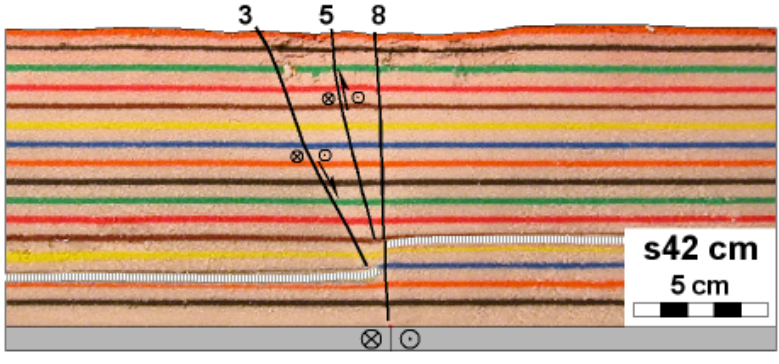
3
5
8
s42 cm
5 cm

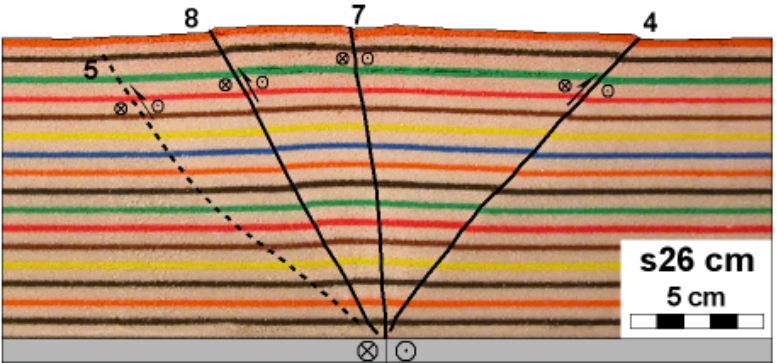
8
7
4
5
s26 cm
5 cm

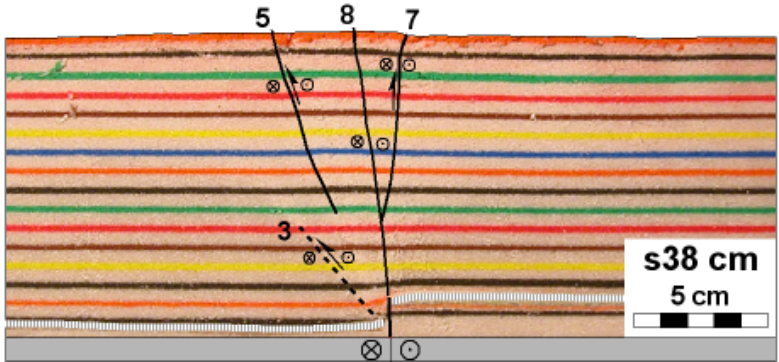
5
8
7
3
s38 cm
5 cm

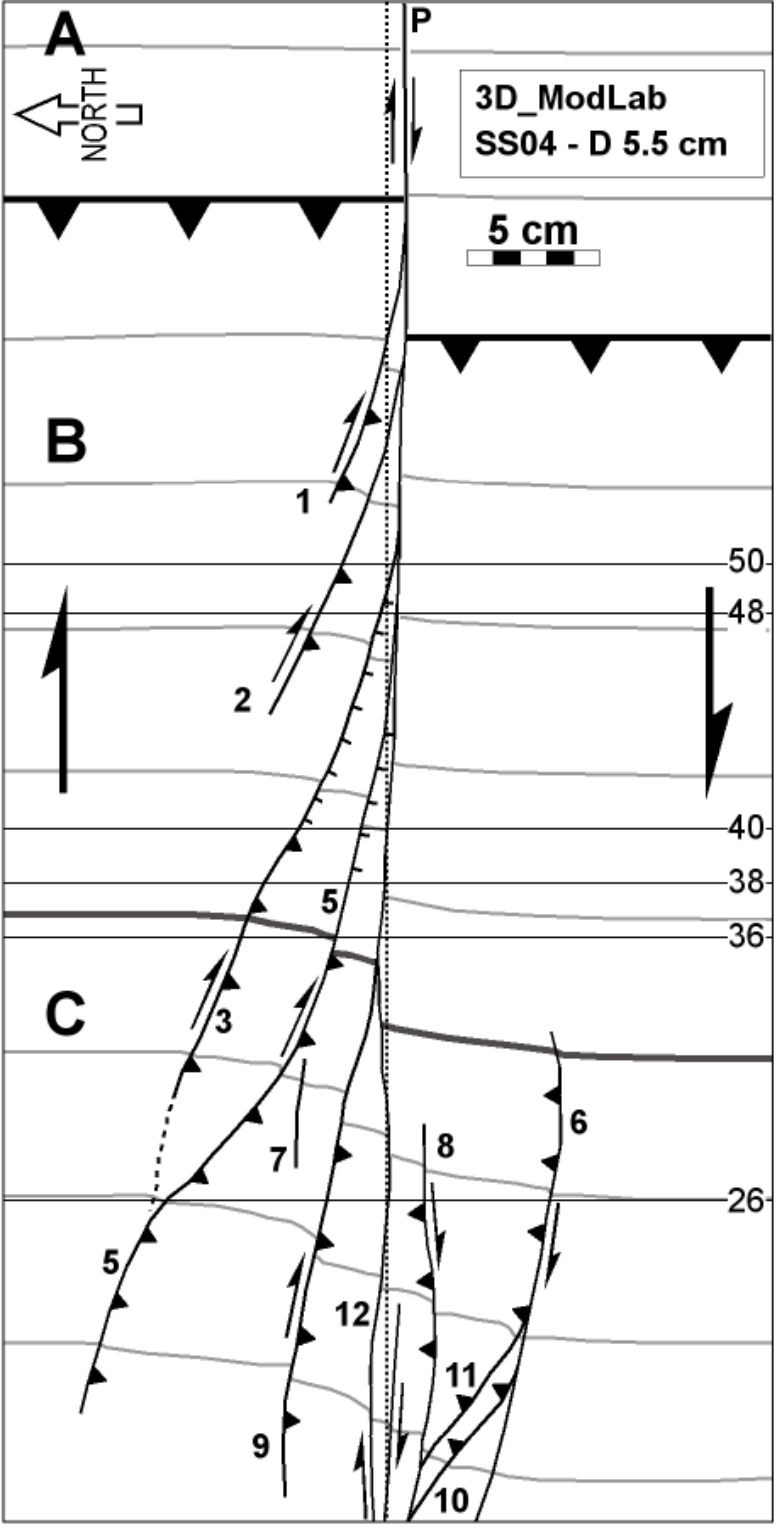
A
NORTH
P
3D_ModLab
SS04 - D 5.5 cm
5 cm
B
1
2
3
5
6
7
8
9
10
11
12
50
48
40
38
36
26
C

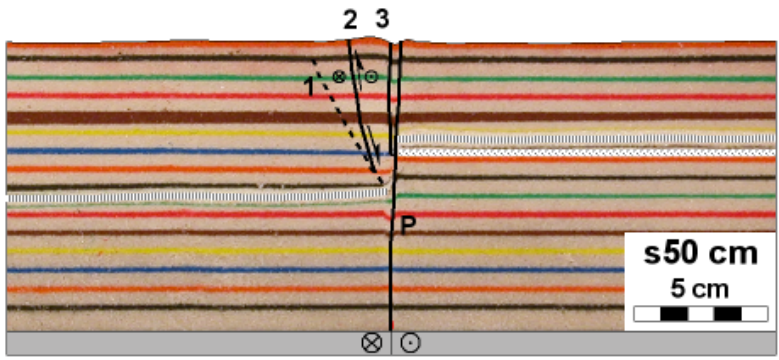
2
3
1
P
s50 cm
5 cm

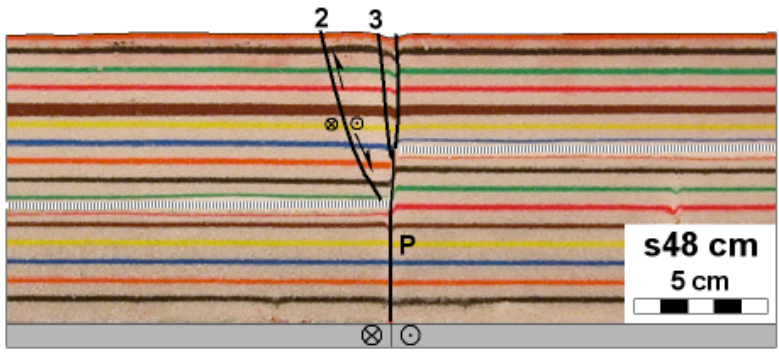
2
3
P
s48 cm
5 cm

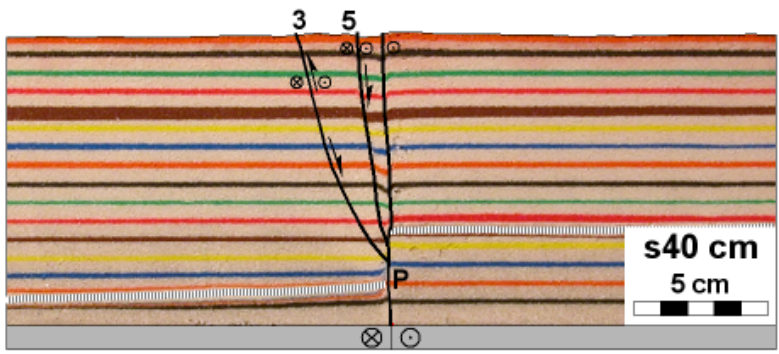
3
5
P
s40 cm
5 cm

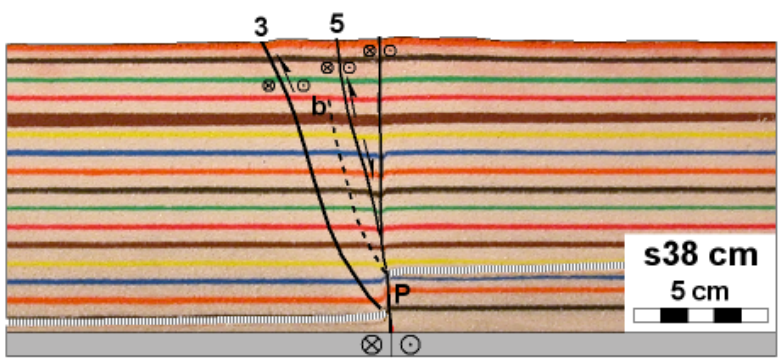
3
5
b
P
s38 cm
5 cm

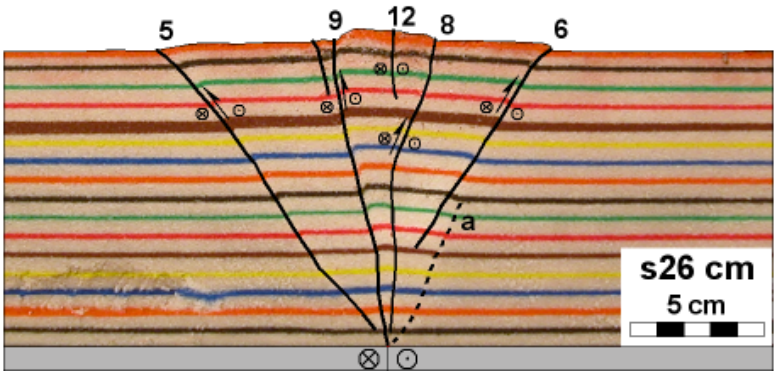
5
9
12
8
6
a
s26 cm
5 cm

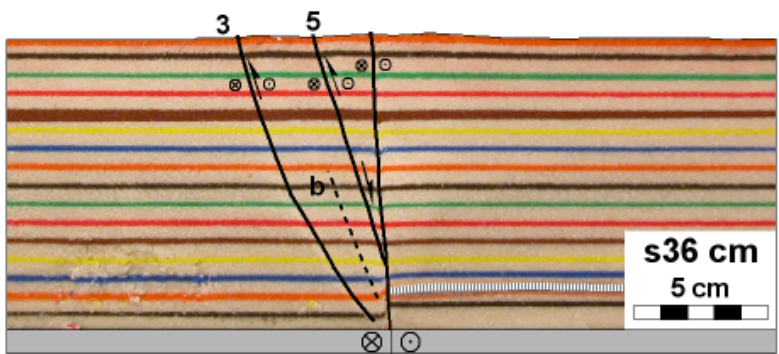
3
5
b
s36 cm
5 cm

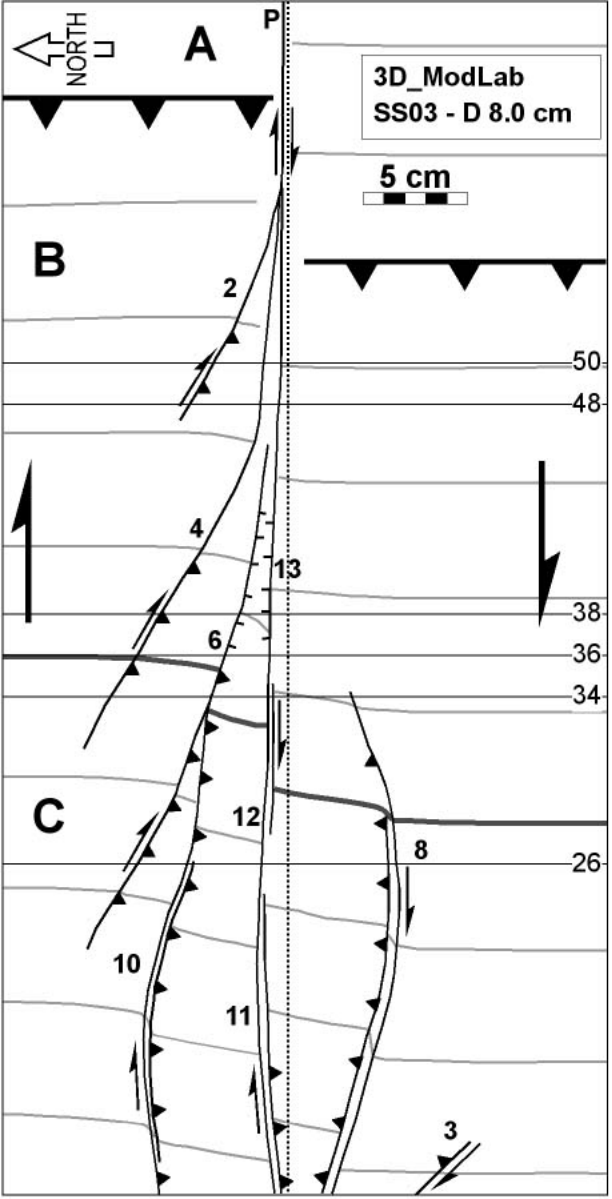
NORTH
A
P
3D_ModLab
SS03 - D 8.0 cm
5 cm
B
2
50
48
4
13
38
6
36
34
C
12
8
26
10
11
3

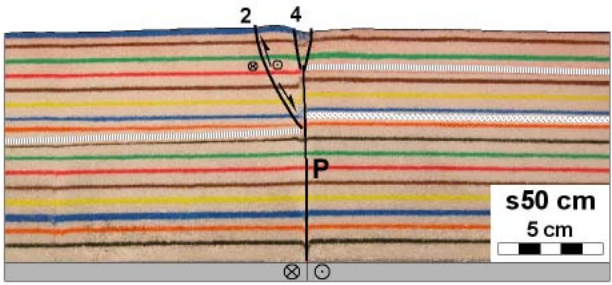
2
4
P
s50 cm
5 cm

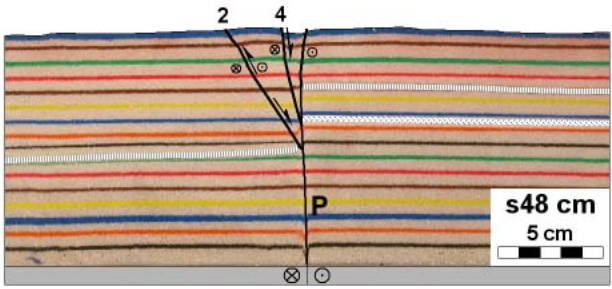
2
4
P
s48 cm
5 cm

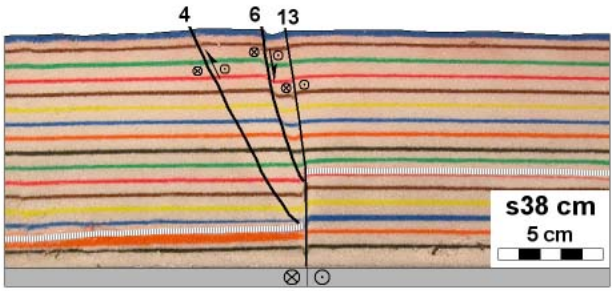
4
6
13
s38 cm
5 cm

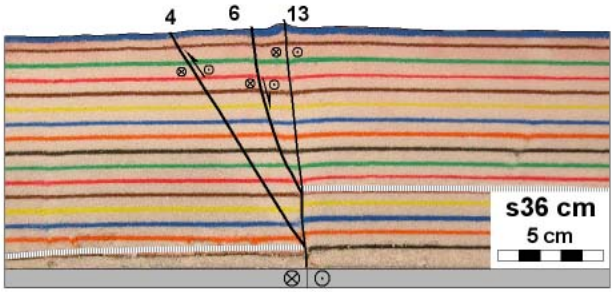
4
6
13
s36 cm
5 cm

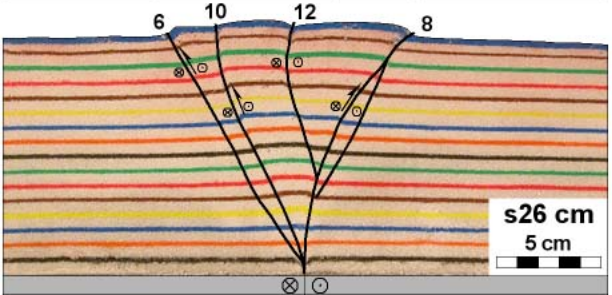
6
10
12
8
s26 cm
5 cm

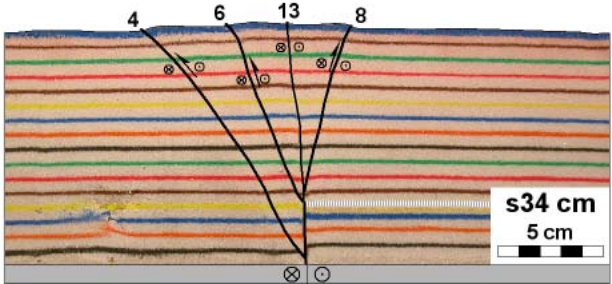
4
6
13
8
s34 cm
5 cm

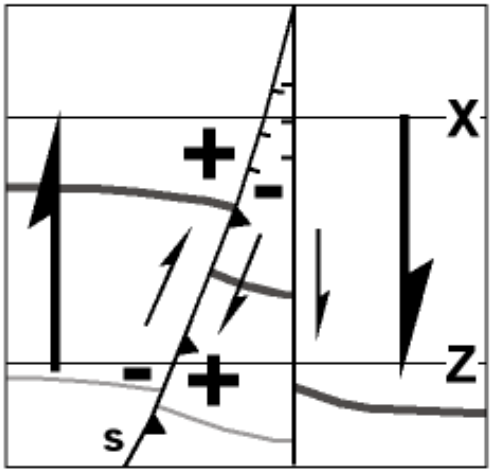
X
Z
s
+
-
-
+

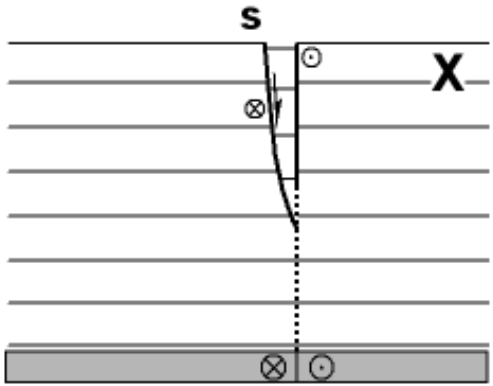
s
X

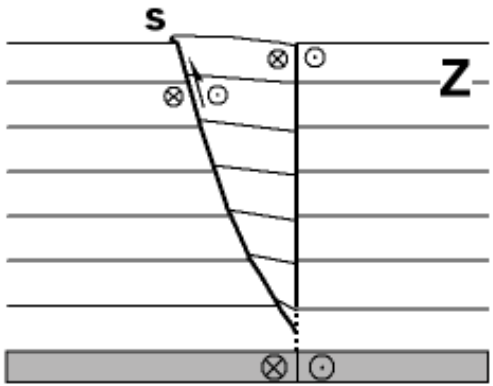
s
Z

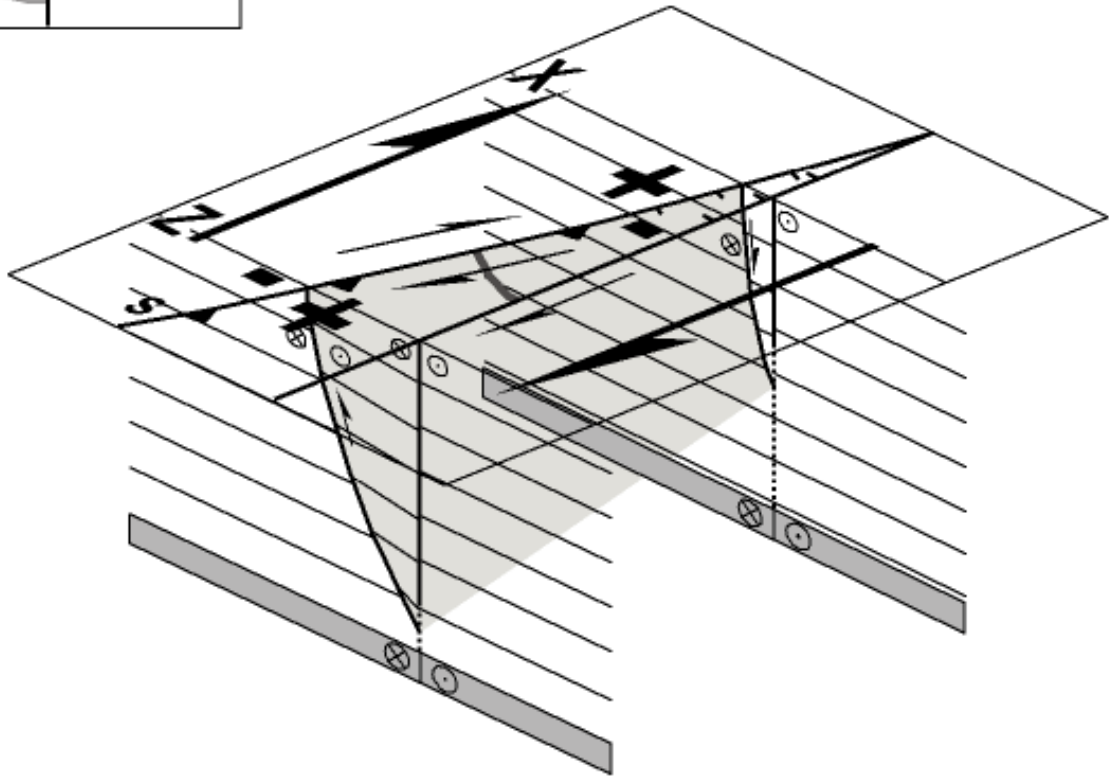
X
Z
s
+
-
-
+

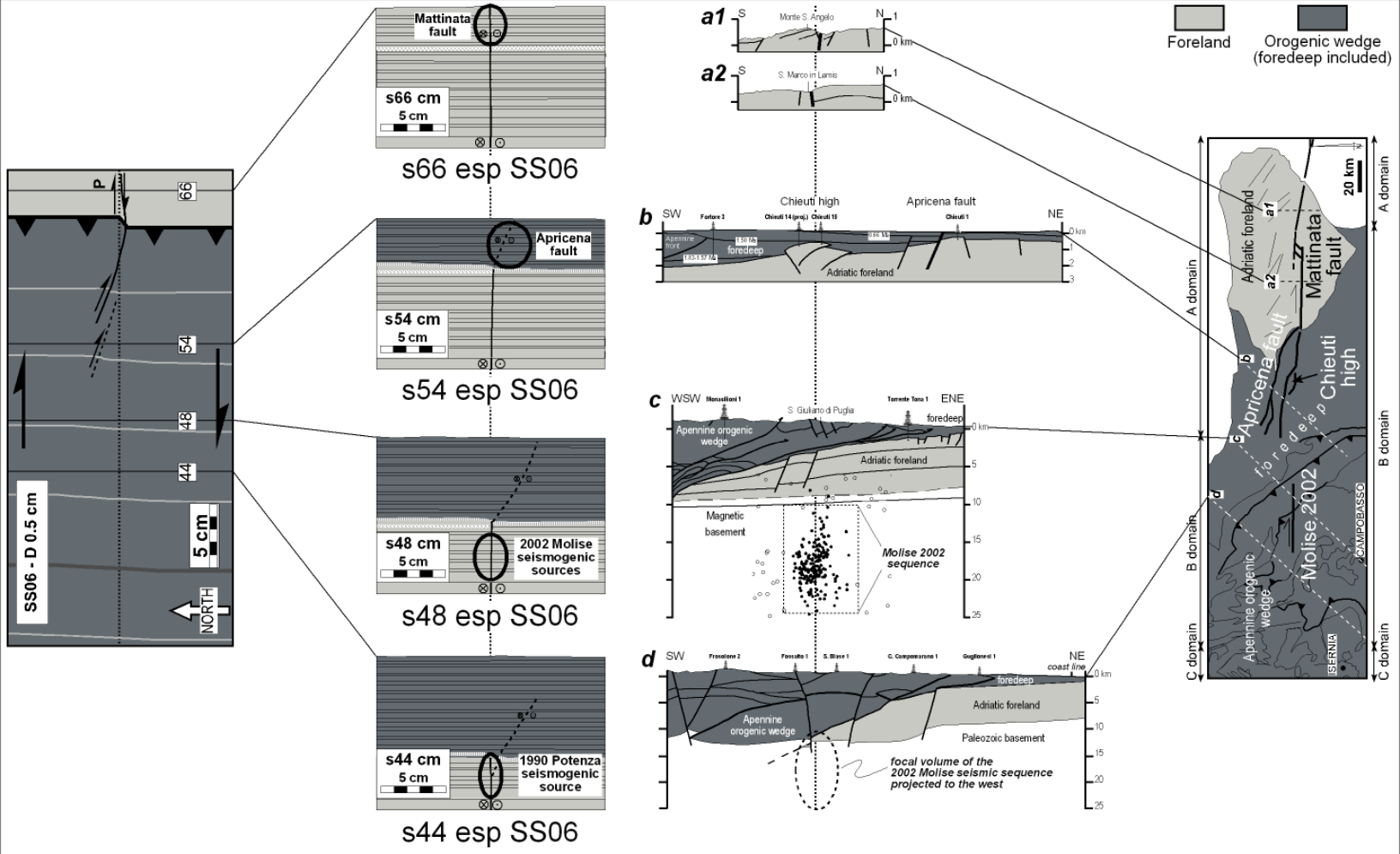
Foreland
Orogenic wedge (foredeep included)
a1
Monte S. Angelo
a2
S. Marco in Lamis
b
Chieuti high
Apricena fault
Adriatic foreland
c
Monsecillani 1
S. Giuliano di Puglia
Torrente Tona 1
Apennine orogenic wedge
Magnetic basement
Molise 2002 sequence
d
Frecalone 2
Fossalto 1
S. Biase 1
C. Campomarano 1
Guglionesi 1
coast line
Paleozoic basement
focal volume of the 2002 Molise seismic sequence projected to the west
Mattinata fault
Apricena fault
Chieuti high
Molise 2002
CAMPOBASSO
ISERNIA
A domain
B domain
C domain
20 km
SS06 - D 0.5 cm
5 cm
NORTH
s66 cm
s54 cm
s48 cm
s44 cm
2002 Molise seismogenic sources
1990 Potenza seismogenic source
s66 esp SS06
s54 esp SS06
s48 esp SS06
s44 esp SS06